Chapter One

Introduction and theory

Introduction

The phenomenon of light scattering by molecules dates back to a derivation of a theory by J.W.Strutt (Lord Rayleigh) in 1899 [1]. Experimental confirmation of this theory was obtained independently by Cabannes [2] and R.J. Strutt [3]. R.J. Strutt also observed that if the incident light was plane polarized then the perpendicularly scattered light was not completely plane polarized. As a result of this work, J.W. Strutt revised the theory [4] to take into account the anisotropy of the molecules present in the gas. The original theory was satisfactory for atoms, such as the noble gases, and for molecules with high symmetry, such as methane, because of the absence of anisotropy in the electronic charge distribution. For molecules of lower symmetry, the revised theory was required.

Pre-laser light-scattering studies used sunlight, carbon arcs and mercury lamps as light sources, with either visual or photographic detection techniques [5]. Unpolarized incident light was used, which gives the depolarization ratio ρ_n rather than ρ_0 and, as shown by Bridge and Buckingham [6], this gives rise to larger geometrical errors. Furthermore, when white light sources were used, the depolarization ratios were average depolarization ratios over the light spectrum. Generally, agreement amongst researchers was poor and the results of these studies have not been considered in this thesis, and certainly they must be viewed with caution.

The development of the laser resulted in remarkable improvements in the

sensitivity of experiments, due to the highly collimated monochromatic light produced. This increased the value of scattering experiments as an analytical tool in the determination of the electric and magnetic properties of molecules. Bridge and Buckingham [6] were the first to use a laser in a light scattering experiment. In their apparatus, the scattering cell was placed inside the laser cavity of a low powered He/Ne laser, resulting in a beam intensity in the cavity of ≈ 0.5 W. The values for the depolarization ratios obtained using this experimental design are still regarded as benchmark figures, due to the remarkable scattering intensities obtained and the small uncertainties which followed. This experimental design is limited because the laser requires retuning when the composition and pressure of the gas inside the laser is changed. With the much higher powered lasers now available, the cell can be placed outside the laser cavity, and the laser will still give sufficient scattering to determine the depolarization ratios to a high degree of precision.

Researchers have used a number of different types of lasers for light scattering experiments. Generally Ar, He/Ne and He/Cd lasers were preferred, due to their stability, tube lifetime and relatively low cost. Rayleigh light scattering experiments were commenced at the University of New England during the latter half of the 1980s, with the aim of studying chemically interesting species and concentrating on vapours rather than gases. The apparatus has been described elsewhere [7], but essentially used a moderately powered He/Ne laser, and a cell positioned outside the laser cavity as the basis for the experimental design.

It is appropriate at this point to define what is actually meant by the term Rayleigh scattering. Molecular scattering consists of vibrational Raman lines and Rayleigh scattering. Rayleigh scattering is composed of a central Cabannes line and rotational Raman lines. The Cabannes line consists of the Landau-Placzek line and the Brillouin doublet [8]. Rayleigh scattering excludes the vibrational Raman lines, since these arise from the interaction of an electric field with the derivatives of the polarizability and not the polarizability itself.

Classical theory of light scattering

The application of a uniform electric field to a molecule results in an induced dipole moment given by [9]

$$\mu_\alpha = \alpha_{\alpha\beta}E_\beta + \frac{1}{2}\beta_{\alpha\beta\gamma}E_\beta E_\gamma + \frac{1}{6}\gamma_{\alpha\beta\gamma\delta}E_\beta E_\gamma E_\delta + \ldots \quad (1.1)$$

where E_β is the electric field, $\alpha_{\alpha\beta}$ is the polarizability, and $\beta_{\alpha\beta\gamma}$ and $\gamma_{\alpha\beta\gamma\delta}$ are the first and second hyperpolarizabilities, respectively. If the electric field strength is low, as in a low powered laser, then the higher order polarizabilities can be ignored and equation 1.1 reduces to

$$\mu_\alpha = \alpha_{\alpha\beta}E_\beta \quad (1.2)$$

This equation assumes that the electric field is uniform over the molecule, which is valid since visible wavelengths are approximately one thousand times larger than molecular dimensions, so that the induced dipole can be treated as a point source.

The classical theory of light scattering is derived from electromagnetic theory, and an outline of a derivation given by Bridge and Buckingham [6] follows. A derivation using the Stokes vector formalism has been given by Barron [10]. Consider a monochromatic polarized electromagnetic wave travelling in the positive Z direction of laboratory-based axes with the electric field vector in the XZ plane incident upon a molecule centred at the origin of the axes (Figure 1.1). The electromagnetic wave induces an oscillating dipole in the molecule which, due to anisotropy of the electronic charge distribution, need not be parallel to the incident electric field.

The mean rate of radiation of this dipole in any direction is given by the Poynting vector [11], which is the vector cross product of the electric and magnetic fields. If an analyzer is placed on the Y axis, where the vector q denotes the orientation of the analyzer, then the steradiance (or mean rate of radiation per unit solid angle) is given by

$$S_0 = \frac{I_0}{(4\pi\varepsilon_0)^2}\left(\frac{2\pi\nu}{c}\right)^4\left(\alpha_{\alpha\beta}q_\alpha e_\beta\right)^2 \quad (1.3)$$

where ν, I_0 and e are the frequency, intensity and direction of the electric field vector of the incident light.

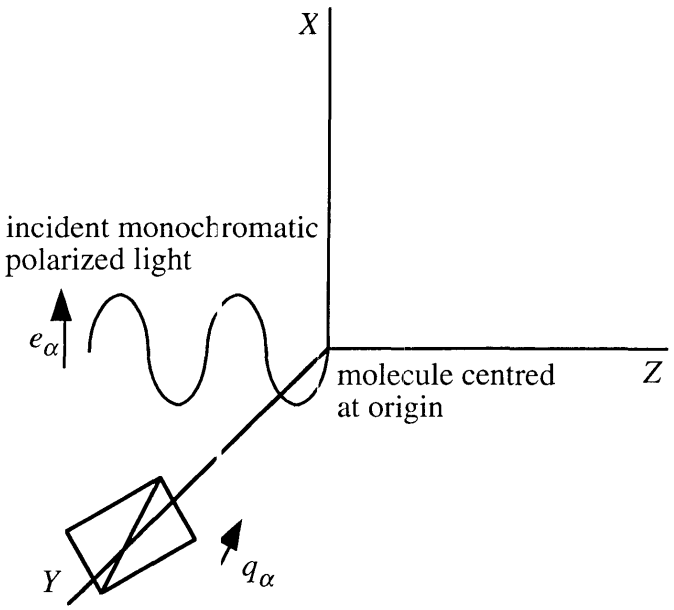

Figure 1.1 Scattering geometry of 90° scattered incident light.

If a molecule-fixed axis system is chosen so that the components of $\alpha_{\alpha\beta}$ are independent of molecular orientation, then the molecular steradiance can be obtained by averaging over all orientations to give the equation

$$\langle S_0 \rangle = \frac{I_0}{(4\pi\varepsilon_0)^2}\left(\frac{2}{c}\frac{\pi\nu}{}\right)^4 \frac{\alpha^2}{5}\left[3\kappa^2 + (5+\kappa^2)\cos^2\theta\right] \qquad (1.4)$$

where θ is the angle between the vectors e_α and q_α. Considering only the steradiance which corresponds to horizontally ($\theta = 90°$) scattered light with respect to the incident light gives

$$I_h = A\frac{\alpha^2}{5}(3\kappa^2) \qquad (1.5)$$

and for vertically ($\theta = 0°$) scattered light

$$I_v = A\frac{\alpha^2}{5}(5+4\kappa^2) \qquad (1.6)$$

where $A = (4\pi\varepsilon_0)^{-2}(2\pi\nu/c)^4 I_0 B$, and B is a factor accounting for the light intensity absorbed by the optical components of the equipment. Therefore, the depolarization ratio is given by

$$\rho_0 = \frac{I_h^v}{I_v^v} = \frac{3\kappa^2}{5+4\kappa^2} \tag{1.7}$$

or upon rearranging,

$$\kappa^2 = \frac{5\rho_0}{3-4\rho_0} \tag{1.8}$$

The polarizability anisotropy parameter, κ, can be related to the various components of $\alpha_{\alpha\beta}$

$$\kappa^2 = \frac{3\alpha_{\alpha\beta}\alpha_{\alpha\beta} - \alpha_{\alpha\alpha}\alpha_{\beta\beta}}{2\alpha_{\alpha\alpha}\alpha_{\beta\beta}} \tag{1.9}$$

For molecules of C_{3v} or higher symmetry, equation 1.9 reduces to

$$\kappa^2 = \left(\frac{\Delta\alpha}{3\alpha}\right)^2 \tag{1.10}$$

where the mean polarizability is given by

$$\alpha = \frac{1}{3}(2\alpha_\perp + \alpha_\parallel) \tag{1.11}$$

since $\alpha_{xx} = \alpha_{yy} = \alpha_\perp$ and $\alpha_{zz} = \alpha_\parallel$ (by convention the z-axis corresponds to the highest-order rotation axis within the molecule). The polarizability anisotropy is defined as

$$\Delta\alpha = \alpha_\parallel - \alpha_\perp \tag{1.12}$$

For molecules with C_{2v} or higher symmetry, equation 1.9 reduces to

$$\kappa^2 = \frac{3\alpha^2 - \alpha_{xx}\alpha_{yy} - \alpha_{xx}\alpha_{zz} - \alpha_{yy}\alpha_{zz}}{3\alpha^2} \tag{1.13}$$

where the mean polarizability is given by

$$\alpha = \frac{1}{3}\left(\alpha_{xx} + \alpha_{yy} + \alpha_{zz}\right) \tag{1.14}$$

At high pressures, the depolarization ratio may have a pressure dependence; a discussion of the theory of pressure-dependent light scattering is delayed until Chapter 3. Generally, at pressures below 100 kPa, the depolarization ratio corresponds to the free-molecule depolarization ratio, ρ_0 [6,12,13].

Quantum theory of light scattering

For a quantum-mechanical treatment of light scattering, it is sufficient to use a semi-classical description, wherein the molecule is quantized and the electromagnetic field is treated classically. Since new theory is not presented in this thesis, only a brief summary of the derivation by Bridge and Buckingham [6] will be given here.

As with the classical derivation, it is assumed that the molecule is small compared to the wavelength of the incident light, so that only the induced electric dipole is significant and non-linear polarization is negligible for the applied field strength. The steradiance given by equation 1.3 is applicable if the polarizability is treated quantum mechanically. If the incident wave of frequency ν travelling in the Z direction has an electric field vector polarized in the X direction, then the steradiance of the scattered light polarized in the direction A is

$$\langle S_{0,A} \rangle = \frac{I_0}{(4\pi\varepsilon_0)^2}\left(\frac{2\pi\nu}{c}\right)^4 \sum_{i,i'}\left(1 - \nu_{i'i}\nu^{-1}\right)^4 n_i |C|^2 \tag{1.15}$$

where

$$C = \sum_{i''}\left[\frac{\langle i|\mu_X|i''\rangle\langle i''|\mu_A|i'\rangle}{h(\nu_{i''i} - \nu)} + \frac{\langle i|\mu_A|i''\rangle\langle i''|\mu_X|i'\rangle}{h(\nu_{i''i'} + \nu)}\right]$$

and n_i is the probability that the mo ecule is in the quantum state ψ_i with energy U_i. The energy difference between the states $\psi_{i''}$ and $\psi_{i'}$ is $h\nu_{i''i'} = U_{i''} - U_{i'}$.

Equation 1.15 can be simplified by separating the internal states ψ_τ (electronic and vibrational) from the rotational states, ψ_R. Since the molecules of interest do not absorb light in the visible region, electronic transitions can be ignored, but transitions giving vibrational Raman lines do occur and must be removed from the scattered light, especially for weakly anisotropic molecules. Experimentally, depolarization ratios below $100\rho_0 \approx 1.5$ usually require the use of a filter to eliminate the vibrational Raman lines. The bandwidth of the filter must be such as to ensure inclusion of all rotational Raman lines associated with the ground electronic and vibrational state of the molecule and exclusion of the vibrational Raman lines.

The steradiances for the O, Q, and S branches of the rotational Raman spectrum of a rigid, linear molecule can be derived with respective frequency factors of $[\nu + 2(2J-1)cB]^4 : \nu^4 : [\nu - 2(2J+3)cB]^4$. If the frequency factors of all three branches are assumed to be ν^4, the steradiances are independent of J and the result is equivalent to the classically derived result of equation 1.4.

The assumption of equivalent frequency factors is questionable only for light molecules such as H_2 and HCl, for which the correction [6]

$$\rho_0 = \frac{3\kappa^2}{5+4\kappa^2}\left(1 - 24cB\nu^{-1} + \ldots\right) \qquad (1.16)$$

can be applied. The contribution to ρ_0 due to changes in the polarizability with rotational and vibrational state as a consequence of non-rigidity of the molecule is small (in the case of rotations) or negligible (for vibrations), even for H_2. Finally, the assumption that $(\nu_{\tau''\tau} - \nu) >> \nu_{R''R}$, where $\nu_{\tau''\tau}$ is the electronic or vibrational transition frequency and $\nu_{R''R}$ is the rotational transition frequency, results in a negligible correction to the depolarization ratio [6].

These quantum corrections have been derived only for small linear molecules, but it is generally accepted that such corrections are likely to be negligible for larger non-

linear molecules. It is assumed in this thesis that the classical theory given by equations 1.4 to 1.14 is applicable if the contribution from vibrational Raman lines is excluded.

Molecular polarizability

From equations 1.7 and 1.10, knowledge of the depolarization ratio and the mean polarizability allows the calculation of the polarizability anisotropy and, in the case of high-symmetry molecules, the polarizability components (equations 1.11 and 1.12). It is important, therefore, to define the polarizability, ascertain the electronic, vibrational and rotational contributions, and indicate experiments that may be used to obtain values of this quantity.

The *ij*-th component of the polarizability in a quantum-mechanical perturbation theory formalism can be written as [14]

$$\alpha_{ij}^{(n)} = \frac{4\pi}{h}\sum_{k}\frac{\omega_{nk}}{\omega_{nk}^2-\omega^2}\langle n|\mu_i|k\rangle\langle k|\mu_j|n\rangle \qquad (1.17)$$

where the molecule is in a non-degenerate quantum state n, and μ_i is the transition dipole moment operator between the states n and k. To avoid resonance effects, the applied optical frequency, ω, is well removed from any electronic transition frequencies, ω_{nk}. Equation 1.17 has been simplified by omitting radiative damping.

The summation over k may be separated into two parts, the sum over vibrational states in the ground electronic state, and the sum over the remaining vibrational states, giving [15]

$$\begin{aligned}\alpha_{ij}^{(0v)} = &\frac{4\pi}{h}\sum_{m}\sum_{u}\frac{\omega_{0v-mu}}{\omega_{0v-mu}^2-\omega^2}\langle 0v|\mu_i|mu\rangle\langle mu|\mu_j|0v\rangle \\ &+\frac{4\pi}{h}\sum_{u}\frac{\omega_{vu}}{\omega_{vu}^2-\omega^2}\langle 0v|\mu_i|0u\rangle\langle 0u|\mu_j|0v\rangle\end{aligned} \qquad (1.18)$$

The first term in equation 1.18 represents the electronic contribution, which may be measured in the visible and ultraviolet regions of the spectrum. The second term is the vibrational contribution, which may be calculated from integrated infrared intensities

[16,17]. The vibrational polarizab lity is a consequence of the distortion by the applied field of the relative position of the nuclei in the molecule. It is zero for atoms and homonuclear diatomic molecules. This contribution may also be zero if the nuclei are held in fixed positions, such as occurs in ab initio calculations, or a dynamic field is applied at a frequency that is high compared to the nuclear vibrational frequencies.

The electronic contribution given by the first part of equation 1.18 is the average polarizability over the ground vibrational state. Computational values must be vibrationally averaged to be directly comparable to the above electronic contribution [18,19]. A third contribution, due to centrifugal distortion from rotational motion, is usually negligible [20]. Finally, allowance must also be made for dispersion in the electronic contribution [21-25]. In this thesis, unless otherwise stated, the experimental mean polarizability, and hence the polarizability anisotropy and polarizability components, are reported at a frequency corresponding to the wavelength of 632.8 nm, and in all cases the mean polarizability refers to the electronic mean polarizability. In some cases it is necessary to compare these values with static computed results obtained from the literature. The computational values reported in this thesis have been corrected to give a dynamic polarizability, but vibrational averaging was not performed.

Several experiments are available to measure the mean polarizability or the anisotropy, and these will be outlined below. The mean polarizability can be related to the refractive index, n, through the well known Lorentz-Lorenz equation [14]

$$\frac{n^2-1}{n^2+2}=\frac{N_A\alpha}{3\varepsilon_0 V_m} \tag{1.19}$$

which at low densities $(n \rightarrow 1)$ becomes

$$n-1=\frac{N_A\alpha}{2\varepsilon_0 V_m} \tag{1.20}$$

Measurement of the refractive index gives the mean optical-frequency polarizability, and there is generally good agreement (approximately 2% maximum deviation) between gas-

and liquid-phase refractive index measurements [12].

Extrapolation of the polarizability to zero frequency gives the static electric polarizability, α^0_{elec}. Addition of the vibrational polarizability α_{vib} [17] gives, indirectly, the overall static polarizability, α^0. This method can also be applied to obtain values of the corresponding polarizability anisotropy, if depolarization ratios at a number of wavelengths are known. The static polarizability can also be obtained directly from measurements of the relative permittivity through the Debye-Clausius-Mossotti equation (for gaseous dipolar species) [14]

$$\varepsilon_r - 1 = \frac{N_A}{\varepsilon_0 V_m}\left[\alpha^0 + \frac{\mu^2}{3kT}\right] \tag{1.21}$$

Mean polarizabilities obtained from measurements of the relative permittivity are usually less accurate than those obtained from refractive index measurements, since account must be taken of the vibrational polarizability.

The static and optical-frequency mean polarizabilities can also be obtained from estimates of the Cauchy moments, otherwise known as dipole sums, given by the equation [26]

$$\alpha(\omega) = \sum_{k=0}^{\infty} S(-2k-2)\omega^{2k} \tag{1.22}$$

where S_{-2} corresponds to the static electric polarizability. The Cauchy moments may be obtained from dipole oscillator-strength distributions by analysis of refractive indices and photoabsorption data [27].

The optical-frequency mean polarizability can also be obtained directly from the Rayleigh light scattering experiment, and a derivation of the relevant equation follows [13]. Given that $\kappa = 0$ for argon, equation 1.6 can be rearranged to give

$$A = \frac{I_v^v(Ar)}{\alpha^2(Ar)} \tag{1.23}$$

Substituting equation 1.23 into equation 1.6 and rearranging gives

$$\alpha = \alpha^2(Ar)\frac{I_v^v}{I_v^v(Ar)}\left(\frac{5}{5+4\kappa^2}\right) \tag{1.24}$$

Substituting equation 1.8 into equation 1.24 gives the expression for the mean polarizability

$$\alpha = \alpha(\mathrm{Ar})\left[\frac{I_v^v}{I_v^v(\mathrm{Ar})}\left(1-\frac{4}{3}\rho_0\right)\right]^{\frac{1}{2}} \tag{1.25}$$

where I_v^v and $I_v^v(\mathrm{Ar})$ are the vertically polarized scattered-light intensities for argon and the species under study, and $\alpha(\mathrm{Ar})$ is the mean polarizability of argon. The method for obtaining values of the mean polarizability with this equation is given in Chapter 2. Mean polarizabilities have been obtained using the above equation in this research but, as will be shown in later chapters, the precision and accuracy are not always high.

The mean polarizability may also depend on temperature. Research by Hohm and Kerl [28,29] on the temperature dependence of the mean polarizability, as reflected in the refractive index, has suggested that an increase in the polarizability with increasing temperature occurs. The effect is small and will not be discussed further in this thesis.

The pressure dependence of the polarizability, as reflected in the refractive index, has been addressed by Buckingham and Graham [30]. The molar refractivity of gases may be expanded as a power series in the molar volume, V_m, giving

$$R_m = \frac{n^2-1}{n^2+2}V_m = A_R + \frac{B_R}{V_m} + \frac{C_R}{V_m^2} + \ldots \tag{1.26}$$

where A_R, B_R and C_R are the refractivity first, second and third virial coefficients. B_R and C_R represent contributions to the molar refractivity from pairs and triplets of molecules. B_R can be measured directly by interferometric techniques [30-32] and is known for only some smaller molecules.

The quadratic Stark effect [14] enables a direct measurement of the static polarizability anisotropy for dipolar molecules from the pure rotational spectrum. For

non-dipolar molecules, molecular-beam measurements may be used to obtain Stark shifts [33]. The R_{20} method can be used to determine the depolarization ratio of a molecule with the vibrational Raman lines excluded. This involves the comparison of the calculated and experimental rotational Raman spectra, which allows evaluation of the ratio [34]

$$R_0 = \frac{\alpha_2^2 + \alpha_{-2}^2}{\alpha_0^2} \tag{1.27}$$

where α_0^2 and $\alpha_2^2 + \alpha_{-2}^2$ are irreducible spherical tensor components of the polarizability.

Of relevance to Rayleigh scattering experiments are the Kerr and Cotton-Mouton effects and the field-gradient birefringence experiment, which are outlined below. The electrooptical Kerr effect measures the birefringence induced in a substance by the application of an electric field. The electric field will partially align the molecules (or atoms) of the sample in the direction of the field by inducing polarization or simply because the molecules are anisotropic. The definition of the molar Kerr constant is [35]

$${}_mK = \frac{6nV_m}{\left(n^2+2\right)^2\left(\varepsilon_r^2+2\right)^2}\left[\frac{n_\parallel - n_\perp}{E^2}\right]_{E=0} \tag{1.28}$$

where ε_r is the relative permittivity, and $n_\parallel$ and $n_\perp$ are the refractive indices parallel and perpendicular to the field, respectively.

The Kerr constant is dependent on molecular interactions within the sample and can be expanded as a virial equation in the molar volume [36]

$${}_mK = A_K + B_K V_m^{-1} + C_K V_m^{-2} + \ldots \tag{1.29}$$

where A_K, B_K and C_K are the Kerr first, second and third virial coefficients. B_K and C_K correspond to interactions between pairs and triplets of molecules, respectively. At very low gas densities ${}_mK = A_K$, since intermolecular interactions are negligible.

A classical derivation of the expression for A_K gives [37]

$$A_K = \frac{N_A}{81\varepsilon_0}\left\{\gamma^K + (kT)^{-1}\left[\frac{2}{3}\mu\beta^K + \frac{3}{10}\left(\alpha_{\alpha\beta}\alpha^0_{\alpha\beta} - 3\alpha\alpha^0\right)\right] + \frac{3}{10}(kT)^{-2}\mu^2(\alpha_{zz} - \alpha)\right\} \quad (1.30)$$

where the z axis is in the direction (negative to positive) of the dipole moment μ, and β^K and γ^K are the mean Kerr first and second hyperpolarizabilities.

The first term in equation 1.30 arises from distortions induced in the substance by the applied field, and the other terms involve orientational effects. For non-dipolar molecules with C_{3v} or higher symmetry, the above equation reduces to

$$A_K = \frac{N_A}{405\varepsilon_0}\left\{5\gamma^K + (kT)^{-1}\Delta\alpha\Delta\alpha^0\right\} \quad (1.31)$$

Therefore, a plot of A_K versus T^{-1} will give γ^K from the intercept and $\Delta\alpha\Delta\alpha^0$ from the gradient. The static polarizability anisotropy, $\Delta\alpha^0$, which includes the vibrational polarizability anisotropy, can be calculated if the optical-frequency polarizability is known. A similar derivation exists for dipolar molecules.

For molecules of C_{2v} or higher symmetry, α_{zz} can be determined by fitting a quadratic to equation 1.30. An alternative method is to rearrange the equation to give

$$\left[A_K - \frac{N_A}{81\varepsilon_0}\gamma^K\right]T = \frac{N_A}{81k\varepsilon_0}\left[\frac{2}{3}\mu\beta^K + \frac{9}{5}\alpha\alpha^0\kappa\kappa^0\right] + \frac{N_A}{270k^2\varepsilon_0}\mu^2(\alpha_{zz} - \alpha)T^{-1} \quad (1.32)$$

which is linearly dependent on T^{-1}, has a gradient that defines α_{zz}, and an intercept that gives β^K. Both methods require knowledge of α, A_K, μ and γ^K. If the information is unavailable, γ^K is usually assumed to be zero.

For isotropic molecules, only the distortion term is non-zero, so that

$$A_K = \frac{N_A}{81\varepsilon_0}\gamma^K \quad (1.33)$$

and A_K is expected to be independent of temperature.

The Cotton-Mouton effect is the magnetic analogue of the Kerr effect, it measures the birefringence induced in a substance by the application of a magnetic field. The Cotton-Mouton constant is determined by measuring the birefringence as a function of the

magnetic induction, B

$$ {}_{\mathrm{m}}C = \frac{2\pi V_{\mathrm{m}}\mu^2}{3(n^2+2)^2}\left[\frac{n_{\parallel}-n_{\perp}}{B^2}\right]_{B=0} \tag{1.34} $$

For a system of non-interacting, diamagnetic, and axially symmetric molecules the Cotton-Mouton constant can be expressed as

$$ {}_{\mathrm{m}}C = \left(\frac{N_{\mathrm{A}}\mu^2}{270\varepsilon_0}\right)\left[\Delta\eta + \left(\frac{2}{3kT}\right)\Delta\alpha\Delta\chi\right] \tag{1.35} $$

where $\Delta\chi$ is the magnetizability anisotropy and $\Delta\eta$ is the magnetic hyperpolarizability anisotropy. There are two contributions to the Cotton-Mouton constant, a temperature dependent effect which depends on $\Delta\alpha$ and $\Delta\chi$, and a temperature independent effect which arises from the anisotropy induced by the magnetic field. A plot of ${}_{\mathrm{m}}C$ against T^{-1} will give $\Delta\eta$ from the intercept and $\Delta\alpha\Delta\chi$ from the gradient. A knowledge of $\Delta\alpha$ from light scattering enables the determination of $\Delta\chi$.

For a rigid, linear molecule a value for the quadrupole moment Θ can be approximated by using the equation

$$ \Delta\chi = \frac{e}{4m_e}\left(\frac{eIg}{m_p} - \Theta\right) \tag{1.36} $$

where I is the moment of inertia and g is the rotational g value (obtainable from molecular-beam magnetic resonance experiments [38]).

The field-gradient birefringence experiment is similar to the Kerr effect except that it measures the birefringence induced in a fluid by the application of an electric field-gradient rather than a uniform electric field. The molar field-gradient birefringence constant, ${}_{\mathrm{m}}Q$, is defined as

$$ {}_{\mathrm{m}}Q = \frac{6n(3\varepsilon_r+2)}{5\varepsilon_r(n^2+2)^2}V_{\mathrm{m}}\left[\frac{n_x-n_y}{E_{xx}}\right]_{E_{xx}=0} \tag{1.37} $$

where E_{xx} is the applied electric field-gradient.

For a linear non-dipolar molecule, the molar field-gradient birefringence constant can be related to the quadrupole moment using the equation

$$_{m}Q = \frac{2N_A}{45\varepsilon_0}\left[\frac{15}{2}B + \frac{\Delta\alpha\Theta}{kT}\right] \tag{1.38}$$

There are two contributions to the molar field-gradient birefringence constant, a temperature dependent effect which depends on $\Delta\alpha$ and Θ, and a temperature independent effect which arises from the quadrupole hyperpolarizability, B. A plot of $_{m}Q$ against T^{-1} will give B from the intercept and $\Delta\alpha\Theta$ from the gradient. A knowledge of $\Delta\alpha$ from light scattering enables the determination of Θ.

Ab initio calculations

The rapid development in the last twenty years of high speed computers and large storage capacity hard disks has revolutionized the contribution of quantum mechanical calculations to chemistry. In particular the ab initio calculation of molecular properties, which was once restricted by the large numerical methods required, is now an excellent tool for investigating these systems. It is now routine for calculations to be performed on small systems with a high degree of accuracy [26,39-43]. The aim of the present study was to use ab initio methods to compare experimental and computational results.

The computations were performed with the CADPAC [44] and GAMESS [45] programs on a DECstation 5000/25, a DECstation 5500 and an Alpha DECstation 3000/800. Since the experimental polarizabilities are frequency dependent, efforts were made to approximate optical-frequency polarizabilities computationally. A description of the basis sets used in this thesis is given in the appendices.

The properties of the molecules were calculated at the Hartree-Fock Self Consistent Field (SCF) level of theory, and Møller-Plesset (MP2) perturbation theory was used to include electron correlation into the calculations. The method of calculating the polarizabilities depended largely on the size and symmetry of the molecule under

investigation. The Coupled Hartree Fock (CHF) [46,47] or the finite-field methods [39,48] were used, and both methods are briefly outlined below.

The finite-field method for calculating polarizabilities involves calculating the energy of the molecule under the influence of an applied electric field. If the applied electric field is small the polarizability can be represented as [39]

$$\begin{aligned}\alpha &= \frac{U(+E)+U(-E)-2U(0)}{E^2} \\ &= \frac{2\{U(E)-U(0)\}}{E^2}\end{aligned} \tag{1.39}$$

or in the case of a molecule possessing a permanent dipole moment

$$\alpha = \frac{U(2E)-2U(E)+U(0)}{E^2} \tag{1.40}$$

The Coupled Hartree-Fock method involves calculating an optimized Hartree-Fock one-determinant wavefunction which is then perturbed to find first-order changes in the orbitals so that self-consistency is achieved in the perturbation. Thus coupling occurs between the perturbation and the electronic charge density of the molecule [49].

Since Version 4 of the CADPAC program was unable to calculate optical-frequency polarizabilities at the MP2 level of theory, these values were estimated from MP2 corrections to the zero-frequency values of the polarizabilities. The difference between the zero-frequency MP2 and SCF values was added to the optical-frequency SCF polarizability values. This resulted in a small error in the polarizabilities, but was assumed to be negligible compared to other approximations inherent in the theory.

Units

The SI system of units is used for the quantities reported in this thesis. Units are given explicity for all quantities, except for polarizabilities where the units of $10^{-40}\,C^2\,m^2\,J^{-1}$ are assumed. Fundamental physical constants used in the analyses were taken from Cohen and Taylor [50]. Unless otherwise stated, frequency-dependent quantities are assumed to be reported at a wavelength of 632.8 nm.

References

1. Strutt, J.W., *Phil. Mag.*, **47**, 375 (1899).
2. Cabannes, J., *Comp. Rend.*, **160**, 62 (1915).
3. Strutt, R.J., *Proc. Roy. Soc. A*, **95**, 155 (1918).
4. Strutt, J.W., *Phil. Mag.*, **35**, 373 (1918).
5. Partington, J.R., *"An advanced treatise on physical chemistry"*, (Longmans, London, 1953).
6. Bridge, N.J. and Buckingham, A.D., *Proc. Roy. Soc. A*, **295**, 334 (1966).
7. Hesling, M.R., *"Measurements of Rayleigh depolarization ratios of gases and vapours."*, Ph.D. Thesis, University of New England, (1990).
8. Young, A.T., *Appl. Opt.*, **20**, 533 (1981).
9. Buckingham, A.D. and Orr, B.J , *Quart. Rev.*, **195**, 21 (1967).
10. Barron, L.D., *"Molecular light scattering and optical activity"*, (Cambridge University Press, Cambridge, 1982).
11. Born, M. and Wolf, E., *"Principles of optics. Electromagnetic theory of propagation, interference and diffraction of light"*, 6th Edition (Pergamon Press, Oxford, 1980).
12. Bogaard, M.P., Buckingham, A.D., Pierens, R.K. and White, A.H., *J. Chem. Soc., Faraday Trans. 1*, **74**, 3008 (1978).
13. Alms, G.R., Burnham, A.K and Flygare, W.H., *J. Chem. Phys.*, **63**, 3321 (1975).
14. Bogaard, M.P. and Orr, B.J , Electric Dipole Polarizabilities Of Atoms and Molecules. In *"MTP International review of science, Physical chemistry"*, Buckingham, A.D. (Ed.), (Butterworths, London, 1975).
15. Cai, W.Q., Gough, T.E., Gu, X.J., Isenor, N.R. and Scoles, G., *Phys. Rev. A*, **36**, 4722 (1987).
16. Whiffen, D.H., *Trans. Faraday Soc.*, **54**, 327 (1958).
17. Bishop, D.M. and Cheung, L.M., *J. Phys. Chem.*, **11**, 119 (1982).
18. Lindh, R. and Liu, B., *J. Chem. Phys.*, **94**, 4356 (1991).
19. Russell, A.J. and Spackman, M.A., unpublished results.

20. Gray, C.G. and Gubbins, K.E., *"Theory of molecular fluids Vol I: Fundamentals"*, (Clarendon Press, Oxford, 1984).

21. Orr, B.J. and Ward, J.F., *Mol. Phys.*, **20**, 513 (1971).

22. Ladanyi, B.M. and Keyes, T., *Mol. Phys.*, **37**, 1809 (1979).

23. Hohm, U., *Mol. Phys.*, **78**, 929 (1993).

24. Hohm, U., *Chem. Phys.*, **179**, 533 (1994).

25. Hohm, U., *Mol. Phys.*, **81**, 157 (1994).

26. Spackman, M.A., *J. Chem. Phys.*, **94**, 1288 (1991).

27. Kumar, A. and Meath, W.J., *Mol. Phys.*, **75**, 311 (1992).

28. Hohm, U. and Kerl, K., *Mol. Phys.*, **58**, 541 (1986).

29. Hohm, U., *Z. Naturforsch.*, **48**, 505 (1993).

30. Buckingham, A.D. and Graham, C., *Proc. Roy. Soc. A.*, **336**, 275 (1974).

31. St Arnaud, J.M. and Bose, T.K., *J. Chem. Phys.*, **68**, 2129 (1978).

32. St-Arnaud, J.M. and Bose, T.K., *J. Chem. Phys.*, **71**, 4951 (1979).

33. Muenter, J.S., In *"MTP International review of science, Physical Chemistry"*, Buckingham, A.D. (Ed.), (Butterworths, London, 1974).

34. Murphy, W.F., *J. Chem. Phys* , **67**, 5877 (1977).

35. Otterbein, G., *Phys. Z.*, **35**, 249 (1934).

36. Gentle, I.R., *"Temperature dependence of the Kerr effect in gases"*, Ph.D. Thesis, University of Sydney, (1987).

37. Buckingham, A.D. and Pople, J.A., *Proc. Phys. Soc. Lond. A*, **68**, 905 (1955).

38. Cederberg, J.W., Anderson, C.H. and Ramsey, N.F., *Phys. Rev.*, **136**, A960 (1964).

39. Werner, H.J. and Meyer, W., *Mol. Phys.*, **31**, 855 (1976).

40. Maroulis, G., *J. Chem. Phys.*, **97**, 4188 (1992).

41. Maroulis, G., *Chem. Phys. Lett.*, **199**, 250 (1992).

42. Maroulis, G., *Chem. Phys. Lett.*, **199**, 244 (1992).

43. Shelton, D.P. and Rice, J.E., *Chem. Rev.*, **94**, 3 (1994).

44. Amos, R.D. and Rice, J.E., CADPAC: The Cambridge Analytic Derivatives

Package. issue 4.0, Cambridge, 1987.

45. Schmidt, M.W., Baldridge, K K., Boatz, J.A., Jensen, J.H., Koseki, S., Gordon, M.S., Nguyen, K.A., Windus, T.L. and Elbert, S.T., *QCPE Bulletin*, **10**, 52 (1990).
46. Dalgarno, A., *Adv. Phys.*, **11**, 281 (1962).
47. Gerratt, J. and Mills, I.M., *J. Chem. Phys.*, **49**, 1719 (1968).
48. Cohen, H.D. and Roothan, C.C.J., *J. Chem. Phys.*, **43**, S34 (1965).
49. Raidy, T.E. and Santry, D.P., *Chem. Phys. Lett.*, **53**, 568 (1978).
50. Cohen, E.R. and Taylor, B.N., *J. Res. Nat. Bur. Stand.*, **92**, 85 (1987).

Chapter Two

Experimental details

Introduction

The first version of the Rayleigh light scattering equipment used in the present research was built in Armidale during the latter 1980s by Dr. M.R. Hesling [1], and since then has undergone a number of alterations to improve the signal-to-noise ratio. The study of vapours, especially, has required significant improvements to the gas and vapour handling system.

A detailed description of the apparatus was given by Hesling [1], and so this chapter includes an overview of the present experimental design and an analysis of only those components that have undergone significant changes. The method of aligning the system is described, a section detailing the method of recording depolarization ratios and mean polarizabilities is included, and a summary of the sources of uncertainties is given.

A description of the light scattering apparatus

During the course of the present research two versions of the Rayleigh light scattering apparatus were used. Version 1 corresponded to the design designated Version 2 in Hesling's thesis; Version 2, as detailed below, incorporated changes to various parts of the system to improve signal strength and stability, and to reduce uncertainties. In the following chapters it is indicated which version of the equipment was used to record the depolarization ratios.

The layout of Version 2 of the experiment is given in Figure 2.1. The radiation

source was a 35 mW laser **L**, which was followed by a half-wave plate **H** to rotate the plane of polarization of the laser light to be vertical rather than horizontal. The light then passed through a polarizer **P** so that only vertically polarized light was selected. Following the polarizer was a chopper **C**, a stop **S1** (diameter 2.4 mm) to reduce the beam scatter, and another larger stop **S4** (diameter 7 mm) mounted within the oven wall. The light then passed through the scattering cell **SC** by means of Brewster angle windows, and then through a stop **S5** (7 mm diameter). Refracted and unscattered light was captured by a Wood's horn **WH** on the outside of the oven.

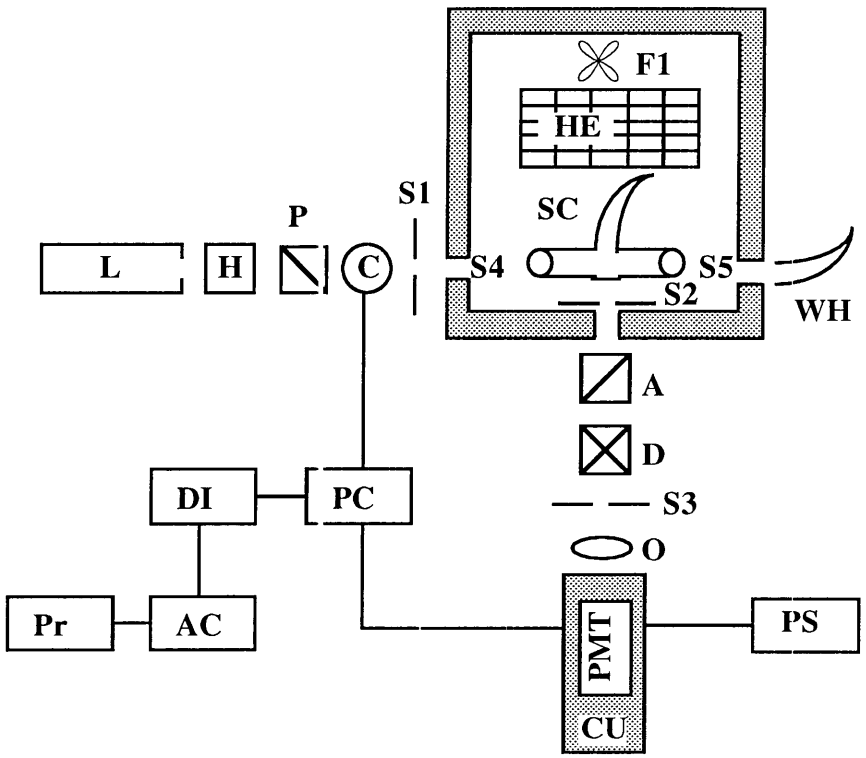

Figure 2.1 Rayleigh light scattering apparatus. **L**, laser; **H**, half-wave plate; **P**, polarizer; **S1**, **S2**, **S3**, **S4**, **S5**, stops; **C**, light chopper; **HE**, heating element; **SC**, scattering cell; **WH**, Wood's horn; **A**, analyzer; **D**, depolarizer; **O**, optical lens; **PC**, photon counter; **DI**, digital interface; **AC**, Apple IIe computer; **Pr**, printer; **PS**, power backup unit; **PMT**, photomultiplier tube; **F1**, fan; **CU**, cooling unit.

The perpendicularly scattered light passed through the exit window, a stop **S2** (diameter 6.35 mm) and then through an analyzer **A**. The function of the analyzer was to

select either the vertically or horizontally polarized light that was scattered from the cell. Following the analyzer was a wedge depolarizer **D** (Special Optics model 80-1025, > 98% depolarization) which was mounted with the analyzer. When required, a 632.8 nm interference filter (Oriel model 52745, diameter 2.54 cm, with a half-height band-width of 12.1 nm) was mounted with the depolarizer to screen out the contribution from vibrational Raman lines of the scattered radiation. Finally, the light passed through a stop **S3**, a lens **O**, two vacuum sealed windows of the cooling unit, and on to the photomultiplier tube **PMT**. The function of the depolarizer was to depolarize the light to eliminate any polarization dependence of the lens **O** and the windows of the photomultiplier cooling unit.

The signal from the photomultiplier tube was passed to a preamplifier (ORTEC/Brookdeal model 9301) and then to the photon counter **PC** (ORTEC/Brookdeal model 5C1). The processed signal from the photon counter passed to a digital-interface **DI** and then to an Apple IIe computer. The photomultiplier tube was a Burle C31034A tube, which had a linear sensitivity from the blue (60 mA W^{-1}) to the red (70 mA W^{-1}), with a quantum efficiency of approximately 12% at 633 nm. The photomultiplier tube was mounted in a Products For Research cooled housing operated at –20 °C. With this design, the dark count across the tube was approximately 400 counts per second (cps) at the normal operating voltage of –1800 V. The original photomultiplier tube power supply (Fluke 412B) was replaced by a Bertan Associates Series 225 power supply.

The photon counter included a synchronous sampler (model 5C21) and a single channel pulse height analyzer (model 5C13). The counter operated with two channels (designated A and B) and one discriminator to select only those counts that were above a certain pulse height (experimentally determined), and also used a window to eliminate pulses that were inordinately high. The counter used a synchronous detection system so that when the chopper was on (allowing the laser light to pass through, position A), the photon counter counted the signal, the dark count and any extraneous radiation. When the chopper was closed (position B), the counter received the dark count and the extraneous radiation. Therefore, by counting A and B synchronously during the same

run, subtraction of A and B resulted in only the signal remaining. Of course this did not exclude scattered radiation from within the cell, which should be minimized in order to obtain a correct depolarization ratio

The Apple IIe computer was programmed to receive both the A and B counts, accumulate them for the period of the run, and calculate the count rate. The program could also control the length and number of count periods in a particular run. The photon counter was triggered by the chopper, but a photodiode, which could be mounted where the Wood's horn was situated, was used to adjust the sampling phase and duty cycle of the photon counter to that of the chopped laser light.

Specific improvements to the experimental design

Below are detailed the specific modifications to the experimental design which improved the stability and reliability of the experiment. Most of the components that comprise the apparatus remained unaltered from the design given by Hesling, and are not detailed here. For example, the main supporting table, the photomultiplier tube housing, the cooling electronics, and the photon counter were not replaced or modified. Optical rails and stands, distances between the optics and stops, mounts for most of the optics, etc. were essentially unchanged.

Laser

The most significant improvement was the replacement of the previous He/Ne laser (Spectra-Physics model 106-1) with a 35 mW He/Ne laser (Spectra-Physics model 127-35). The laser operated in the TEM_{00} mode with horizontal polarization of greater than 500 : 1; this required the addition of a half-wave plate to rotate the plane of polarization by 90°. The beam diameter was 1.25 ± 0.10 mm compared with 0.68 ± 0.02 mm for the model 106-1. The 35 mW laser was at least three times the length and weight of the smaller 10 mW laser and major structural changes were made to the laser support stands to reduce vibration and misalignment of the laser. A 1.5 m railing was installed to accommodate the new laser and this required a new strut to support the weight of the railing.

The support stands were screwed directly into the casing of the laser. The brass stands consisted of beams with dimensions 125 x 25 x 9 mm attached to threaded rods of length 120 mm and diameter 19 mm. The rods were also sheer on one side to enable a pinning screw to hold the rod securely within the optical mount, which reduced vibrations and the possibility of displacement of the laser. Nuts were used on each threaded rod to provide vertical movement, and a second locking nut was included for stability. These mounts provided greater stability and ease of alignment than the previous mounts which supported the 10 mW laser.

Half-wave plate

The half-wave plate (Newport model 10RP12-24) was placed after the laser on a precision rotator (Oriel model 13011). This rotator allowed the plate to be aligned to within 0.1° of the vertical using a nulling technique detailed later in this chapter.

Chopper

The light chopper (Stanford Research Systems model SR540) was used with frequencies of between 70 and 100 Hz; the manufacturer's data indicated that long-term frequency drift was less than 2%. Previous versions of the apparatus relied on a photodiode placed where the Wood's horn was positioned to trigger the photon counter, and this invariably contributed to background noise because of light reflection back into the cell. The chopper had an internal signal which triggered the photon counter, therefore it was possible to replace the photodiode with the Wood's horn. In fact it is noted that the small exit window of the scattering cell could be replaced by a Wood's horn, rather than having the Wood's horn externally mounted on the oven wall. Knowledge of the position of the exiting laser beam on the exit window, however, greatly assisted in the alignment of the cell and the laser.

Positioner

The cell was held in position with a right-hand *XYZ* positioner (Newport Ultralign M-561-XYZ) which had a left-hand tilt mount attached (M-561-TILT-LW). This replaced the simple Cajon fitting that previously held the cell. A modified chemical clamp was screwed into the top of the positioner to allow firm clamping of the scattering

cell. This allowed quick alignment of the cell and small adjustments in the cell's position when required. The addition of the 35 mW laser resulted in greater sensitivity of the depolarization ratio to the position of various components of the equipment. The addition of the positioner to allow precise movements reduced the time required to align the cell accurately, and allowed rapid minimization of the internal spuriously scattered light.

Power backup unit

The photomultiplier tube housing was connected to a Total Power Systems SPS 550 power backup unit. This unit provided approximately fifteen minutes backup time on a full load of 440 W. The cooled housing drew around a quarter of the full load and thus the backup time was extended to approximately one hour. The backup unit provided a safety net in case the power failed, otherwise the housing required drying out overnight in an oven at 40 °C.

Analyzer

A new analyzer (Newport 10GTO4AR.14) was installed after the first prism failed. It was thought that the failure was due to heat stress caused by the temperature differential between the external and oven temperatures (the prism was mounted inside a tube that protruded into the wall of the oven). The analyzer was mounted between two sections of tubing (50 mm and 45 mm) by means of threads on the outside of the analyzer casing and on the inside surface of the tube sections, and the sections were held securely to the analyzer with a grub screw. The 50 mm length of tube then protruded into the wall of the oven with the other end of the combined tubing attached to a micrometer-drive system, as detailed by Hesling. The result of this modification was to shift the location of the prism further away from the heat of the oven by approximately 20 mm thereby reducing the heat stress. An other benefit of this design was that the prism could be easily removed for cleaning, if required, simply by unscrewing the two sections of tubing. The previous design glued the prism within the tubing, making replacement or cleaning difficult.

Gas and vapour handling system

Previous studies of Rayleigh light scattering naturally tended to investigate species that are gaseous or are highly volatile at room temperature. The aim of the present research was to study chemically interesting species that have reasonable vapour pressures at approximately 90 °C. A description of the gas and vapour handling system is given in Figure 2.2, and the reader is referred to previous designs [1,2] for comparison.

The styrofoam insulation of the oven was replaced by fibreglass insulation (ACI duct lining, 25 mm thickness) covered with high temperature paint to reduce fibre dust. This increased the maximum operating temperature of the oven from 90 to 150 °C. The stops **S4** and **S5** were mounted within the oven walls to reduce encroachment of the insulation into the path of the laser beam. The stops also served to minimize extraneous light and aid in the alignment of the laser.

It is stressed that 150 °C is an optimistic assessment of the maximum operating temperature of the main oven. Although temperatures of 120 °C were used in the present research (Chapter 8), the limiting component of the system was the plastic fan (labelled **F1** in Figure 2.1) within the main oven. This fan provided an even temperature distribution but failed at temperatures above ≈ 110 °C due to the material of manufacture.

All the tubing was standard 6 mm stainless steel tubing, which reduced the possibility of chemical reactions occurring with the gases and vapours. **V1**, **V2** and **V3** were bellows valves (Nupro SS-4BK-VP) of stainless steel construction and had removable high temperature Viton o-rings (SS-4BGO-K5-T, with insert SS-4BA-K5).

T1, **T2** and **T3** were three-way ball valves (Whitey SS-42XS4) of stainless steel construction. **T1** was attached to the vacuum pump below the oven, and permitted evacuation of the sample from the top or bottom of the cell. **V3** allowed the tubing inside the oven to be isolated from the external plumbing. This kept all the components at the same temperature and avoided pressure variations throughout the tubing; this proved to be a significant improvement to the reliability and stability of the system. **V1**, **V2** and **T1** were attached to a removable aluminium sheet (500 mm long, 240 mm wide, 2 mm thick) which enabled cleaning without requiring a complete rebuild of the system.

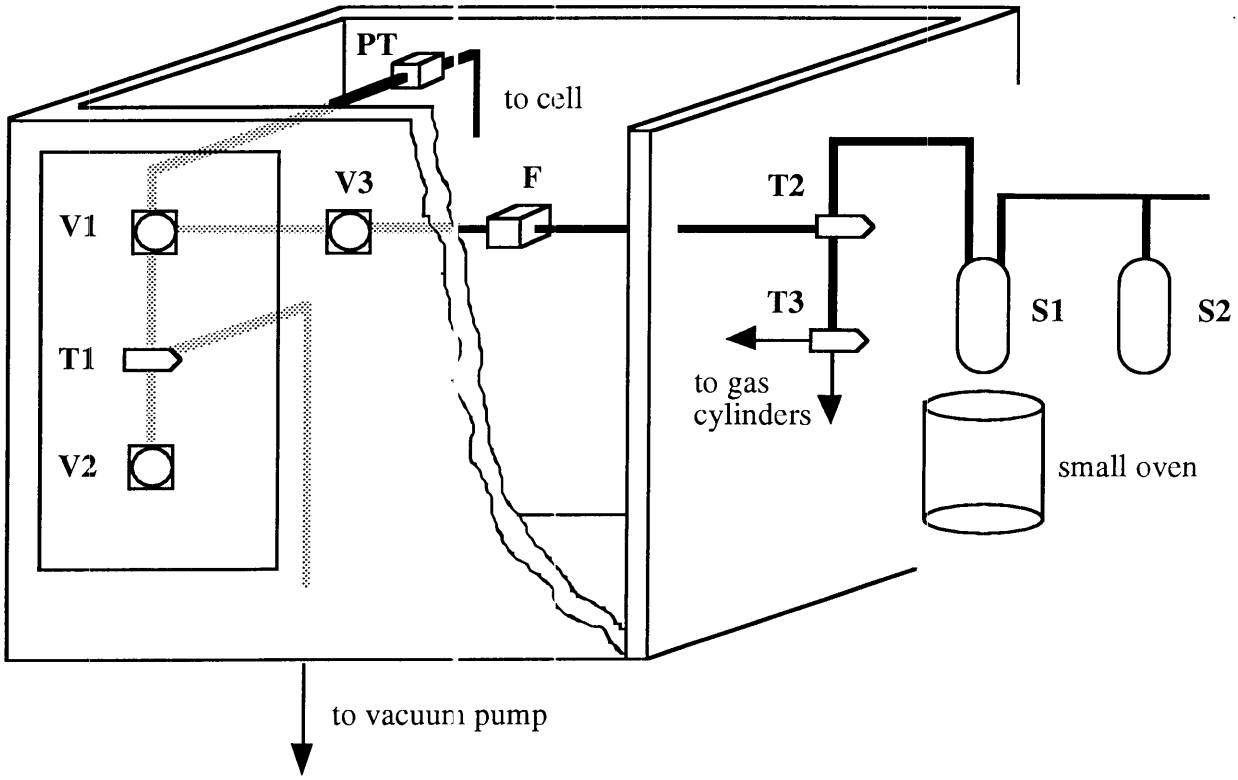

Figure 2.2 Gas and vapour handling system. **V1**, **V2** and **V3** are bellows valves, **T1**, **T2** and **T3** are three-way valves and **S1** and **S2** are sample tubes. **F** is a dust filter and **PT** is a pressure transducer The laser is situated behind the oven and the photomultiplier tube is located to the left of the picture.

Although new cells were fabricated, the design followed that given by Hesling and will not be detailed here. The cell was attached to the gas and vapour handling system using flexible tubing (Cajon 321-4-X-4 with inserts 304-4-XOA) and Cajon fittings on each end. The Cajon fittings required Viton o-rings (Ludowici BS-010). Similarly, the Brewster angle windows were attached to the cell using brass Cajon fittings with o-ring seals (Ludowici BS-114). Most of the connections, however, were simple Swagelok fittings. The filter **F** (Nupro SS-4TF) contained 0.5 μm pores which reduced the possibility of dust entering the cell. In some cases, a second filter of the same type was installed to aid elimination of dust. The pressure was monitored by a pressure transducer **PT** (Data Instruments SA25A), which was accurate to at least four significant figures, although this was limited by pressure fluctuations along the tubing.

The external tubing was wrapped in heating tape (Sephco KPG75) and then insulated with fibreglass insulating tape, although in later work plumber's insulation (safe to ≈ 100 °C) was used; the heating tape was then connected to a Variac. One aim of the new design was to reduce the quantity of fibreglass tape required by mounting most of the gas and vapour handling system within the oven.

A significant improvement was to replace the Variacs that controlled the two ovens with dedicated temperature controllers. The heating element within the oven was controlled by a West 2071 temperature controller, and this provided stable temperatures for indefinite periods of time with variations of less than half a degree. The temperature of the small oven was maintained by a Eurotherm controller (model E2780), although the stability of this oven was not important as long as the temperature of the sample was within a range suitable for entry of the heated sample into the main oven. Temperatures within the plumbing system and the ovens were qualitatively monitored with Type K thermocouples connected to a selector switch (RS 332-969) and digital display (RS 258-186). The actual temperature of the main oven was recorded with a full immersion thermometer placed in the top of the oven and located approximately 10 cm from the cell. The thermometer had an accuracy of greater than 0.05 °C.

The general procedure when performing experiments on vapours was to fill the sample bottle **S2** with the liquid and then freeze-pump-thaw. The sample was then distilled over to **S1** and again freeze-pump-thawed. Thus the sample was subjected to two freeze-pump-thaw cycles, and this was adequate to remove any dissolved gases. **S1** could then be isolated from **S2** and surrounded by the small oven to pre-heat the sample in preparation for filling of the scattering cell.

General alignment procedure

The sensitivity of the apparatus to the position and orientation of various optical components increased upon the introduction of the 35 mW laser. This resulted in a slightly different procedure for aligning the equipment than that given by Hesling.

The laser was aligned to be horizontal using aligning posts. These were brass

posts with dimensions 120 x 12 x 2 mm with horizontal holes (diameter = 1.20 ± 0.05 mm), situated 5.00 ± 0.05 mm from the top of the post. The posts were mounted in magnetic blocks by means of screw threads. The laser was set to be approximately horizontal by ensuring the beam passed through the two stops located in the entrance and exit walls of the oven (**S4** and **S5** in Figure 2.1). The aligning posts were situated approximately 2 m from the laser, with a 1 m long level balanced on top (a smaller, more accurate level was usually placed on top of the 1 m level). The aligning posts were supported by laboratory jacks which enabled the posts to be moved vertically. Precise alignment of the laser entailed moving the jacks so that the level indicated it was horizontal, then moving the optical stands of the laser so that the beam passed through the horizontal holes of the aligning posts.

The procedure for the alignment of the half-wave plate was as follows. A travelling microscope containing cross-hairs in the eye-piece was placed parallel to the exiting laser beam. The cross-hairs were rotated to be horizontal by focusing on a level. The cross-hairs were then focused on a polarizer with a known fast axis, and the fast axis was rotated to be parallel with the horizontal line of the cross-hairs. The half-wave plate was then placed on the optical rail immediately following the laser. If the fast axis was horizontal, then rotating the half-wave plate to minimize the intensity of laser light through the polarizer resulted in rotating the incident laser light through 90°. This method was then independent of any slight tilt in the laser. A second polarizer was then placed in the optical system following the half-wave plate, and rotated until its fast axis was crossed with the first polarizer. The incident polarized light should then be completely polarized in the vertical direction.

Once the half-wave plate and polarizer were aligned, the cell was placed in the positioner which was bolted to the oven floor. The cell was then aligned by sight using the adjustment screws of the positioner to minimize the scattered laser light within the cell. At this point exact alignment was not crucial since a fine adjustment was made later. The cell was then repeatedly flushed with carbon dioxide and then filled.

The analyzer, depolarizing wedge, chopper and lens were then put in place. The

photomultiplier tube was aligned by determining the count rate over 100 s for carbon dioxide as a function of its horizontal and vertical position. A maximum corresponded to the optimum position. Various stops were also aligned by this method as well, if they were suspected of interfering with the main beam.

The analyzer was aligned by measuring the signal obtained from carbon dioxide using integration times of 100 s. The maximum and minimum count rates were roughly located using trial and error, and then accurately obtained by rotating the analyzer mount by 1° turns and determining the count rate. The maxima and minima corresponded to the polarized and depolarized positions of the analyzer, and were so marked. It remained only to put all covers and stops in place, and determine the depolarization ratio of carbon dioxide. Fine adjustment of the position of the scattering cell usually resulted in the correct depolarization ratio for carbon dioxide of $100\rho_0 = 4.01$.

Although the method of alignment was relatively simple, it was an extremely demanding task requiring repeated measurements of the depolarization ratio of carbon dioxide, and alignment of the various components, before a satisfactory ratio was obtained. Without a precisely aligned system any experimental results were worthless, and it was thought prudent not to use a scaling technique. For example, if the carbon dioxide depolarization ratio was $100\rho_0 = 4.08$, then the ratio for another molecule could be scaled down by 1.7%. Scaling has not been determined to be a satisfactory solution to the frustrating situation of having a slightly high or low depolarization ratio for carbon dioxide. The main concern was that scaling was not directly transferable over large changes in the scattered light intensity resulting from changing the gas or vapour samples. The general procedure was to ensure that the depolarization ratio for carbon dioxide was accurate before examining other species.

Nitrogen, acetylene and benzene vapour were used to ensure the linearity of the photon counting system when subjected to large changes in light intensities and depolarization ratios. Therefore, results for these species provided a secondary check on the consistency and stability of the system, and of the method of recording depolarization ratios.

Method of analysis

Depolarization ratios

The general method of obtaining a depolarization ratio was to count the polarized background, $I_{v,b}^{v}$, fill the cell with the gas or vapour and allow the pressure to equilibrate, and then count the polarized component, I_{v}^{v}. The analyzer was then rotated by 90° so that only the depolarized light was selected, and the depolarized component, I_{h}^{v}, was counted. Finally, the gas was evacuated from the cell and the depolarized background, $I_{h,b}^{v}$, was counted. Subtraction of the background signals using equation 2.1 gave the depolarization ratio.

$$\rho_0 = \frac{I_h^v - I_{h,b}^v}{I_v^v - I_{v,b}^v} \qquad (2.1)$$

This is only one method of determining the depolarization ratio, but it resulted in only one rotation of the analyzer during the course of a ratio. Another method of determining the depolarization ratio involved recording the count rate as a function of gas density for both the polarized and depolarized components of the analyzer (usually ten gas densities were used for both components). The count rates were plotted against the gas density and the ratio of the gradients of the lines gave the depolarization ratio. The limitations of the pressure-dependent ratio method were the availability of virial coefficients for the conversion of pressures into gas densities, the errors associated with the least-squares analysis, and the recording of a ratio generally taking four times longer than by the method described above

Mean polarizabilities

During the course of the present research efforts were made to determine the mean polarizability for each compound. The main restrictions for a determination of the mean polarizability were the availability of a sufficient pressure range and reasonable pressure stability. Therefore, mean polarizabilities of the heavier vapours such as boron tribromide and tribromomethane were not recorded. In such cases, literature values as determined by the experiments outlined in Chapter 1 were used.

The mean polarizability was determined with equation 1.25, where the optical-frequency (632.8 nm) mean polarizability of argon is defined in this thesis as $\alpha(\mathrm{Ar}) = 1.851 \pm 0.002$. This was derived from the mean of the values given by Kumar and Meath [3] and Hohm and Kerl [4]. The method involved recording the polarized scattered light intensities of argon and the species under investigation as a function of pressure; generally ten pressures were used for both samples. The pressures were converted to number densities, with account taken of the non-ideality of the gases if virial coefficients were available. Linear least-squares analyses were performed on the plots of count rate against gas density to obtain, in terms of the gradients of the lines, the values of I_v^v and $I_v^v(\mathrm{Ar})$ required for equation 1.25. Since a determination of the mean polarizability with this method required at least four hours, only one value was recorded for each gas or vapour, although there were some exceptions. In cases where the presence of a laser line filter resulted in a significant reduction in the depolarization ratio, then the filter was also used in the determination of the mean polarizability.

A systematic study has not been done on this method of determining the mean polarizability. However this thesis does provide a number of preliminary studies on the precision and accuracy of the mean polarizability so determined, and also the effect of a laser line filter. The general conclusion of these studies (refer to the results for carbon dioxide, fluoroethane and hexafluoro-2-butyne) was that the values obtained with this method are not as reliable as values obtained from measurements of the refractive indices. In most cases where there was a disagreement between mean polarizabilities obtained by the two methods, the refractive indicies were usually of greater accuracy, or assumed to be so.

Sources of uncertainties

Imperfections and misalignments of the optical components give rise to a number of uncertainties, and these have been addressed in detail by Hesling [1]. The problem of divergent incident and scattered light was solved by Bridge and Buckingham [5] and only a summary of their conclusions is given in this section.

The Rayleigh depolarization ratio of 90° scattered light can be written in the Stokes vector formalism as [6]

$$\rho_0 = \frac{S_0^d + S_1^d}{S_0^d - S_1^d} \tag{2.2}$$

where S_0^d and S_1^d correspond to real parts of the Stokes parameters of the 90° scattered light. Upon substituting values for S_0^d and S_1^d, equation 2.2 can be written as [1]

$$\rho_0 = \frac{6\beta(\alpha)^2}{45\alpha^2 + 7\beta(\alpha)^2 + \left[45\alpha^2 + \beta(\alpha)^2\right]P\cos 2\eta\cos 2\zeta} \tag{2.3}$$

where $\beta(\alpha)^2 = \left(3\alpha_{\alpha\beta}\alpha_{\alpha\beta} - \alpha_{\alpha\alpha}\alpha_{\beta\beta}\right)/2$ and $\alpha^2 = \alpha_{\alpha\alpha}\alpha_{\beta\beta}/9$. P, η and ζ are the degree of polarization, the ellipticity and the azimuth, respectively, of the incident light. Substituting $1 + \sigma = P\cos 2\eta\cos 2\zeta$ into equation 2.3 gives

$$\rho_0 = \frac{6\kappa^2}{10 + 8\kappa^2 + \sigma\left(5 + 4\kappa^2\right)} \tag{2.4}$$

which for perfectly polarized incident light ($\sigma = 0$) is equivalent to equation 1.5.

If the azimuth of the transmission axis of the polarizer is at an angle ζ to the vertical then unless $\zeta = 0$ the laser light is not completely polarized. Equation 2.4 describes the effect of $\zeta \neq 0$ upon the observed depolarization ratio. Hesling has shown that the error introduced into the depolarization ratio from this source is < 0.002% when $\rho_0 \approx 1 \times 10^{-2}$ and < 0.004% when $\rho_0 \approx 1 \times 10^{-3}$.

The entrance and scattering windows of the cell contained small retardances (maximum 20 μrad). Application of Mueller calculus, which describes a linear retarder, to the Stokes vector of a perfectly linear polarized light beam gives the equation [1]

$$S = \sin 2\rho \sin\varphi \tag{2.5}$$

where ρ is the azimuth of the fast axis, φ is the relative retardance of the linear retarder, and S is the fourth Stokes parameter of the light after passing through the retarder.

The ellipticity, η, introduced into a polarized beam when passed through a linear retarder is [7]

$$\eta = \frac{1}{2}\sin^{-1} S \tag{2.6}$$

For a relative retardance of φ = 20 μrad, η = 0.0006°, and the value of σ in equation 2.4 is negligible. Therefore, slight retardance of the entrance window results in a negligible effect on the observed depolarization ratio. The effect of the retardance of the scattering window was also shown by Hesling to be negligible.

The effect upon the observed depolarization ratio of a misaligned analyzer can be described by the equation [1]

$$\rho_0 = \frac{3\varepsilon^2 + (5+\kappa^2)\cos^2\theta_1}{3\varepsilon^2 + (5+\kappa^2)\cos^2\theta_2} \tag{2.7}$$

where $\theta_1 \approx 90°$ and $\theta_2 \approx 0°$; this corresponds to polarized and depolarized positions of the analyzer respectively. Hesling has shown that the analyzer can be set in each position to better than 0.17°, the error introduced is < 0.09% for ρ_0 = 1 x 10^{-2}, and < 0.9% for ρ_0 = 1 x 10^{-3}.

If β is the angle of divergence of the incident light beam, then the observed depolarization ratio is [5]

$$(\rho_0)_{obs} = \rho_0 + \frac{1}{4}B^2 \tag{2.8}$$

where $0 \le \beta \le B$, and B is the maximum divergence defined by a stop placed in the incident beam. The beam divergence of the 35 mW He/Ne laser is β = 0.66 ± 0.06 mrad. The error from this source is 1.1 x 10^{-7}, so for ρ_0 = 1 x 10^{-2} the error is < 0.002%, and for ρ_0 = 1 x 10^{-3} the error is < 0.02%.

For divergent scattered light the maximum divergence accepted by the detector is C $(0 \le \gamma \le C)$, where γ is the angle of divergence of the scattered light. The observed depolarization ratio is given by

$$(\rho_0)_{obs} = \rho_n \left(1 + \frac{1}{4}C^2\right) + \frac{1}{24}C^4 + \ldots \qquad (2.9)$$

where Hesling determined the divergence angle to be $\gamma < 6°$. This introduces errors of < 0.4% and < 0.8% into ratios of $\rho_0 = 1 \times 10^{-2}$ and 1×10^{-3}, respectively.

A negligible error arises from a slight deviation of the polarization vector of the laser beam to the horizontal plane [1]. The uncertainties outlined above are only first order effects; second order effects are assumed to be negligible, since there is excellent agreement with other researchers for the depolarization ratios of well studied species such as benzene, carbon dioxide and nitrogen. In the above analyses it has been assumed that uncertainties are not compounded.

References

1. Hesling, M.R., *"Measurements of Rayleigh depolarization ratios of gases and vapours."*, Ph.D. Thesis, University of New England, (1990).
2. Stankey, R., *"Anisotropic polarizabilities of aliphatic molecules"*, M.Sc. Thesis, University of New England, (1991).
3. Kumar, A. and Meath, W.J., *Can. J. Chem.*, **63**, 1616 (1985).
4. Hohm, U. and Kerl, K., *Mol. Phys.*, **69**, 803 (1990).
5. Bridge, N.J. and Buckingham, A.D., *Proc. Roy. Soc. A*, **295**, 334 (1966).
6. Barron, L.D., *"Molecular light scattering and optical activity"*, (Cambridge University Press, Cambridge, 1982).
7. Shurcliff, W.A., *"Polarized light, production and use"*, (Harvard University Press, Cambridge, Massachusetts, 1962).

Chapter Three

Carbon dioxide, carbonyl sulfide and carbon disulfide

Introduction

The electric and magnetic properties of carbon dioxide, carbonyl sulfide and carbon disulfide have been much studied both experimentally and theoretically. Some recent experiments include gas-phase Kerr effect [1-4], gas-phase Cotton-Mouton effect [5,6], and gas-phase field-gradient birefringence experiments [7,8]. Various other refractivity [9-11] and Stark effect [12,13] measurements have been reported. A precise dipole moment for carbonyl sulfide has also been reported [14]. Carbon dioxide has been extensively studied computationally [15], but most of the calculations have neglected electron correlation. Recent work on these molecules includes a configuration-interaction calculation for carbonyl sulfide by de Brouckère *et al.* [16], SCF polarizability calculations on carbon disulfide by Maroulis [17], and fourth-order many-body perturbation theory calculations by Maroulis and Thakkar [15]. For the series of molecules, Spackman [18] has calculated MP2 polarizabilities with the 6-31G(+sd+sp) basis set, and Russell and Spackman [19] have calculated ground state vibrationally averaged properties to the MP2 level of theory using the MPOL1 basis set.

The depolarization ratios of carbon dioxide, carbonyl sulfide and carbon disulfide have been determined by several researchers [20,21]. In the present research, carbon dioxide was the molecule of choice for checking the equipment due to its unusually high ratio, availability, stability and purity. A correct determination of the depolarization ratio

of carbon dioxide was essential in gauging the accuracy of the apparatus, as was discussed in Chapter 2. Furthermore, there is some disagreement amongst the literature values for carbonyl sulfide and carbon disulfide. This chapter reports the depolarization ratios and mean polarizabilities for carbon dioxide and carbonyl sulfide, and resolves the discrepancy amongst the values of the depolarization ratios reported for carbon disulfide.

Experimental details

Carbon dioxide was obtained from CIG Ltd (> 99.95%) and was sublimed to remove dust. Carbonyl sulfide was obtained from Matheson Gas Products (> 97%), and was used without further purification. Carbon disulfide was obtained from BDH Ltd (> 99.9%) and was purified following a procedure given in the literature [22]. Gas-chromatographic analysis of carbon disulfide gave a final purity of > 99.99%.

All the ratios were recorded using Version 2 of the equipment. For carbon dioxide at 25 °C and ≈ 100 kPa, typical polarized and depolarized counts were 12 897 and 520 cps, with background counts of 12 and 3.5 cps, respectively. For carbonyl sulfide at 25 °C and ≈ 100 kPa, polarized and depolarized counts were 97 189 and 3 787 cps, with background counts of 26 and 8.6 cps. Integration times for carbon dioxide were 200 s for the depolarized component and 100 s for the polarized component; the integration times were doubled for carbonyl sulfide.

Since carbon dioxide was the gas used to calibrate the experiment, numerous ratios have been recorded. From experience, ratios of $100\rho_0 = 3.99 \pm 0.03$ (vibrational Raman lines excluded) and $100\rho_0 = 4.01 \pm 0.03$ (vibrational Raman lines included) have been chosen as the most reliable. As was shown by Bridge and Buckingham [23], this indicates that the vibrational Raman contribution to the depolarization ratio is too small to be precisely determined for ratios of this size. Seven mean polarizabilities were recorded for carbon dioxide to investigate the magnitude of the mean polarizability and the precision of the equipment; the results are given in Table 3.1. Also included in Table 3.1 are the seven depolarization ratios recorded for carbonyl sulfide with inclusion of the vibrational Raman lines. One mean polarizability was recorded for carbonyl sulfide,

giving a value of α = 5.95 ± 0.03 The method of Pitzer [24] was used to calculate virial coefficients for carbonyl sulfide giving, B(296 K) = −302.7 x 10^{-6} m^3 mol^{-1} and B(298 K) = −298.4 x 10^{-6} m^3 mol^{-1}; other virial coefficients were obtained from Dymond and Smith [25].

Table 3.1 Mean polarizabilities for carbon dioxide and depolarization ratios for carbonyl sulfide.

$\alpha(CO_2)$	$100\rho_0$(OCS)
2.978 ± 0.004[a]	3.857 ± 0.005
2.936 ± 0.005[a]	3.917 ± 0.005
2.988 ± 0.007[a]	3.945 ± 0.005
2.943 ± 0.003[a]	3.928 ± 0.005
2.983 ± 0.005	3.889 ± 0.005
2.975 ± 0.003	3.909 ± 0.005
2.969 ± 0.004	3.879 ± 0.005

[a] Vibrational Raman lines excluded.

From Table 3.1, it can be seen that the precision of the experiment for recording the mean polarizability of carbon dioxide was satisfactory, although there was some variation in the mean polarizabilities which excluded the vibrational Raman lines. The precision is also discussed in Chapter 6 for fluoroethane, and Chapter 7 for hexafluoro-2-butyne. The depolarization ratios given in Table 3.1 for carbonyl sulfide are satisfactory. A laser line filter was not used since the ratio was large enough for the vibrational Raman contribution to be negligible. Summaries of the present results are given in Tables 3.4 and 3.5, together with theoretical and experimental literature values. The mean polarizability for carbon dioxide quoted in Table 3.4 is given as the mean of the seven polarizabilities, regardless of whether the vibrational Raman lines were included or excluded.

The depolarization ratio for carbon disulfide is not accurately known. The literature values of $100\rho_0 = 7.18 \pm 0.07$ for 632.8 nm [21], $100\rho_0 = 7.41 \pm 0.07$ for 647.1 nm [20], and $100\rho_0 = 7.3 \pm 0.2$ for 632.8 nm [26] are clearly in poor agreement. A preliminary investigation of the depolarization ratio of carbon disulfide gave ratios ranging from 7.06 to 7.33, depending on the pressure. It was evident that the depolarization ratio for carbon disulfide had a remarkably high pressure dependence, even within the range of pressures below ≈ 100 kPa.

Following the preliminary investigation, the measurements were repeated, taking extreme care in the recording of the ratios. Typical polarized and depolarized counts for 25 °C and ≈ 40 kPa gave 77 516 and 5 408 cps, with background counts of 38 and 6 cps, respectively. The polarized counts were not unusually high (see boron trichloride in Chapter 4), and therefore a non-linear intensity dependence of the photomultiplier tube response was eliminated. Pulse pile-up errors were assumed to be negligible, since the pulse-height analyzer had a pulse-pair resolution of 10 ns [27]. Ratios were recorded with Version 2 of the experiment, with integration times of 100 s for the polarized component and 200 s for the depolarized component. The depolarization ratios recorded in the present research are given in Table 3.2 together with the corresponding pressures. The ratios as a function of the number density are given in Figure 3.1. Density second virial coefficients for conversion of pressures to number densities were obtained from the literature [25].

From Figure 3.1, it can be seen that there is a definite pressure dependence of the depolarization ratio of carbon disulfide. The quality of the data was reduced at higher densities where signals became noisy, presumably due to triplet and higher interactions. At low densities integration times were tripled to reduce the uncertainties. The error bars in Figure 3.1 are the photon-counting statistics of each ratio.

The density dependence of the depolarization ratio of carbon dioxide was also investigated, although from the results of Dayan *et al.*[28], the present study was unlikely to observe an effect within the pressure range up to ≈ 100 kPa; Dayan *et al.* used pressures up to ≈ 100 MPa. The resulting ratios are given in Table 3.3 and are also

plotted in Figure 3.2. Extreme care was taken in recording the data, with integration times of 1 000 s for the depolarized component, and 500 s for the polarized component. Runs were not performed until complete pressure stabilization was achieved. Even with the greatest care and patience, it is evident from Figure 3.2 that the pressure dependence of the depolarization ratio of carbon dioxide was negligible over the pressure range available.

Table 3.2 Pressure dependence of the depolarization ratio of carbon disulfide.

Pressure (kPa)	100ρ	Pressure (kPa)	100ρ
39.38	7.014 ± 0.010	18.27	7.202 ± 0.014
37.15	7.053 ± 0.010	17.18	7.200 ± 0.015
35.43	7.012 ± 0.010	16.41	7.210 ± 0.015
35.38	6.972 ± 0.010	14.84	7.231 ± 0.016
33.60	7.068 ± 0.010	13.59	7.246 ± 0.018
31.85	7.041 ± 0.010	13.01	7.258 ± 0.017
31.60	7.138 ± 0.010	11.04	7.294 ± 0.019
29.84	7.134 ± 0.011	9.84	7.256 ± 0.021
28.06	7.097 ± 0.011	9.28	7.318 ± 0.021
27.63	7.036 ± 0.011	7.52	7.309 ± 0.024
25.51	7.110 ± 0.012	6.34	7.342 ± 0.027
24.57	7.103 ± 0.012	5.71	7.318 ± 0.023
23.94	7.127 ± 0.012	3.70	7.417 ± 0.030
22.33	7.154 ± 0.012	2.66	7.349 ± 0.048
20.89	7.123 ± 0.013	2.01	7.394 ± 0.045
20.28	7.162 ± 0.013	1.57	7.478 ± 0.071

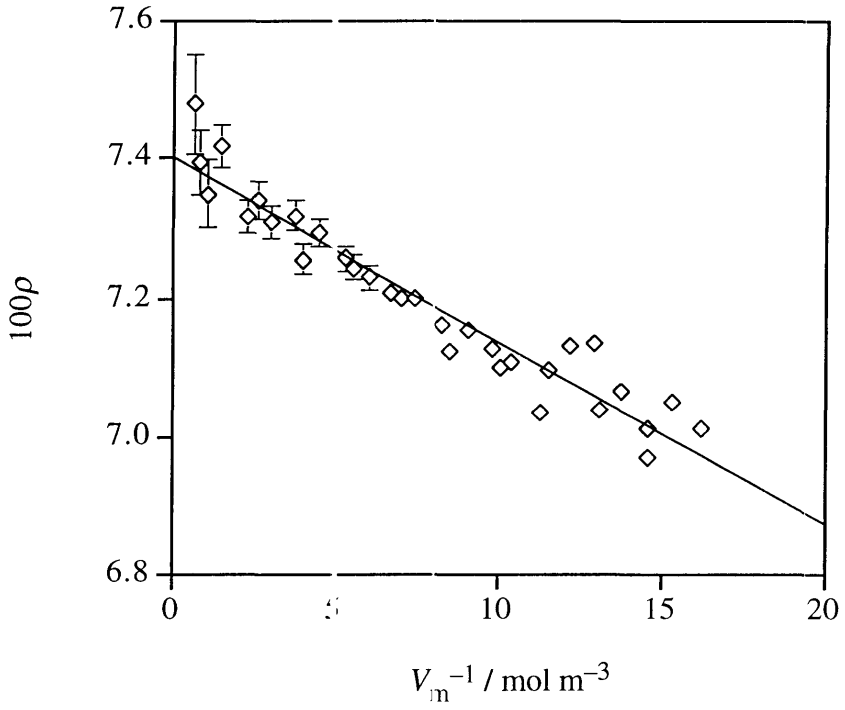

Figure 3.1 Depolarization ratio of carbon disulfide as a function of number density.

As mentioned in Chapter 2, the depolarization ratio can also be obtained by recording the polarized and depolarized components as a function of the number density, and taking the ratio of the gradients of the subsequent plots to be the depolarization ratio. This procedure is generally not favoured due to the length of time required to record the ratio and because of the uncertainties introduced during the least-squares fitting procedure [27]. A depolarization ratio for carbon dioxide was recorded using the above method giving the plots in Figures 3.3 and 3.4 and a ratio of $100\rho_0 = 4.02 \pm 0.02$. This agreed with the single pressure depolarization ratios recorded during the same period.

Using the same method for carbon disulfide, however, gave ratios of $100\rho_0 = 7.08 \pm 0.09$ and $100\rho_0 = 7.00 \pm 0.08$, and the plots for the first ratio are given in Figures 3.5 and 3.6. Clearly, this method is inapplicable for molecules such as carbon disulfide, which have strong intermolecular interactions. Caution must then be exercised in the interpretation of the accuracy of the mean polarizability for carbon disulfide determined in the present study, since the procedure is similar to the above method for obtaining the depolarization ratios.

Table 3.3 Pressure dependence of the depolarization ratio of carbon dioxide.

Pressure (kPa)	100ρ
93.21	4.001 ± 0.008
71.82	4.026 ± 0.010
50.62	4.008 ± 0.013
22.20	4.051 ± 0.023
15.18	4.040 ± 0.036

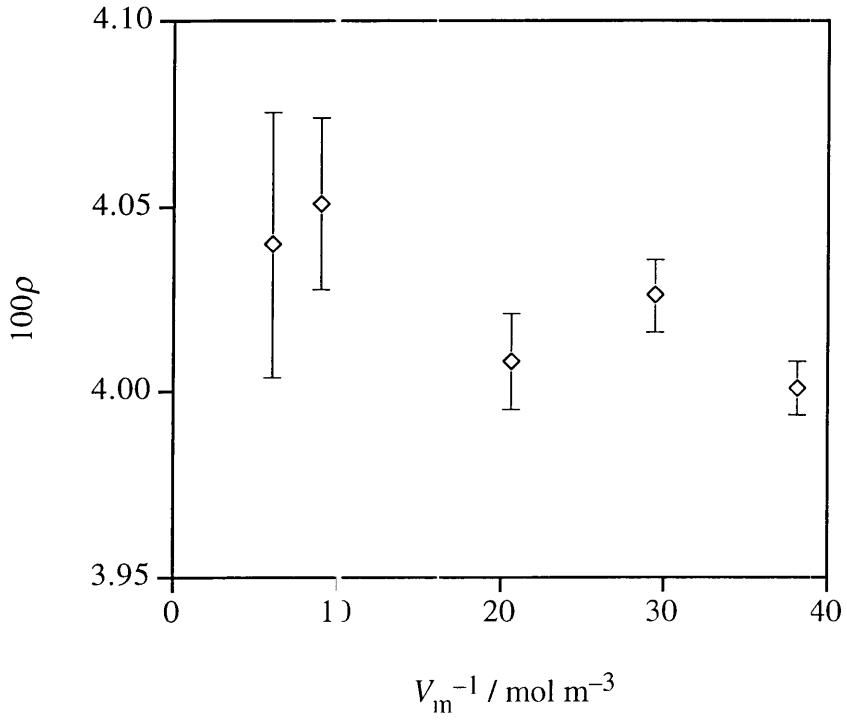

Figure 3.2 The depolarization ratio of carbon dioxide as a function of number density.

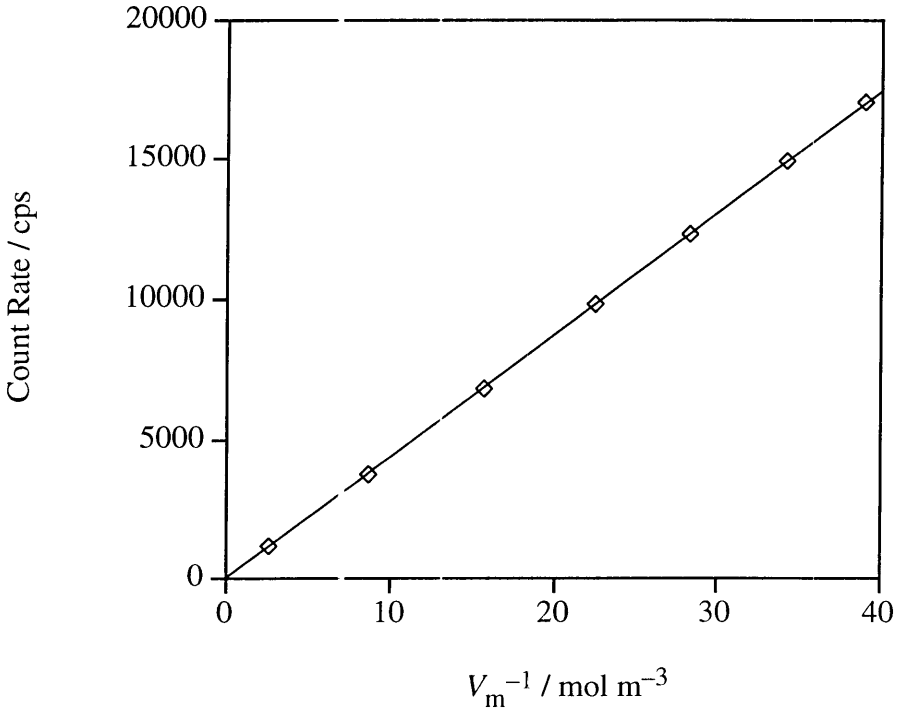

Figure 3.3 Polarized count rates as a function of number density for carbon dioxide.

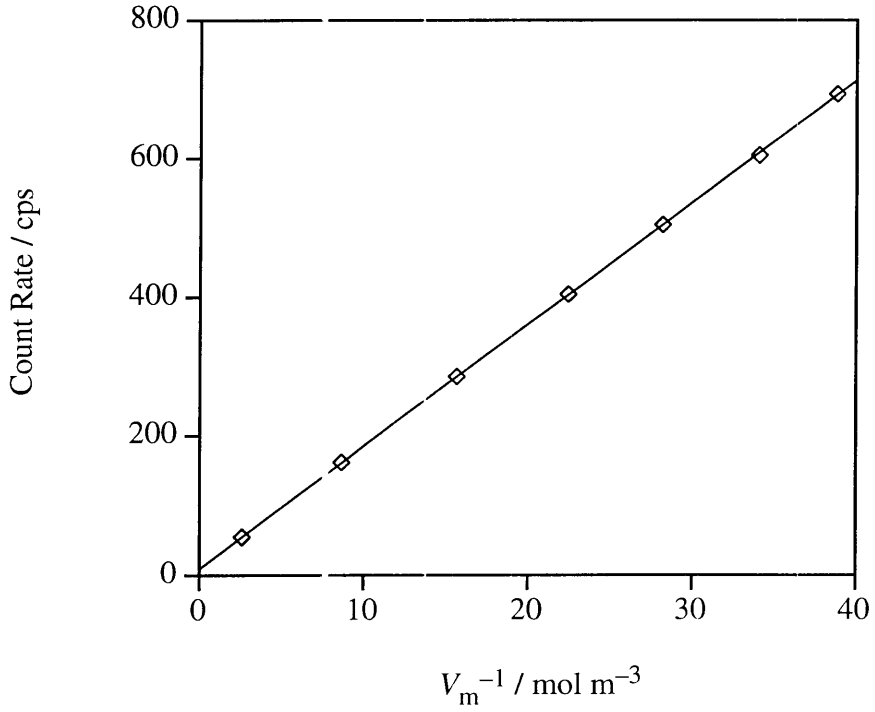

Figure 3.4 Depolarized count rates as a function of number density for carbon dioxide.

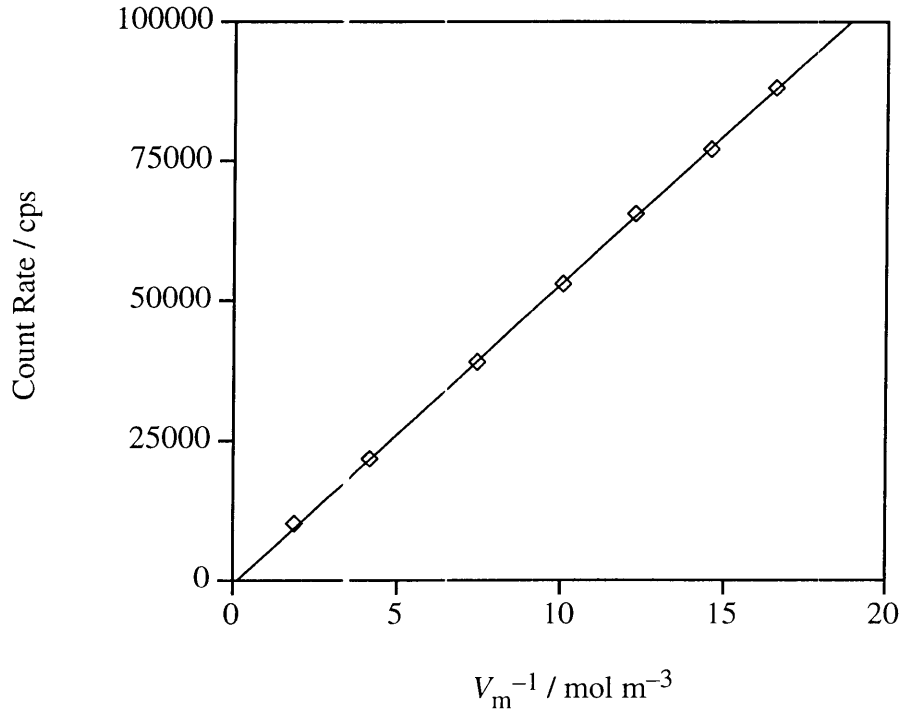

Figure 3.5 Polarized count rates as a function of number density for carbon disulfide.

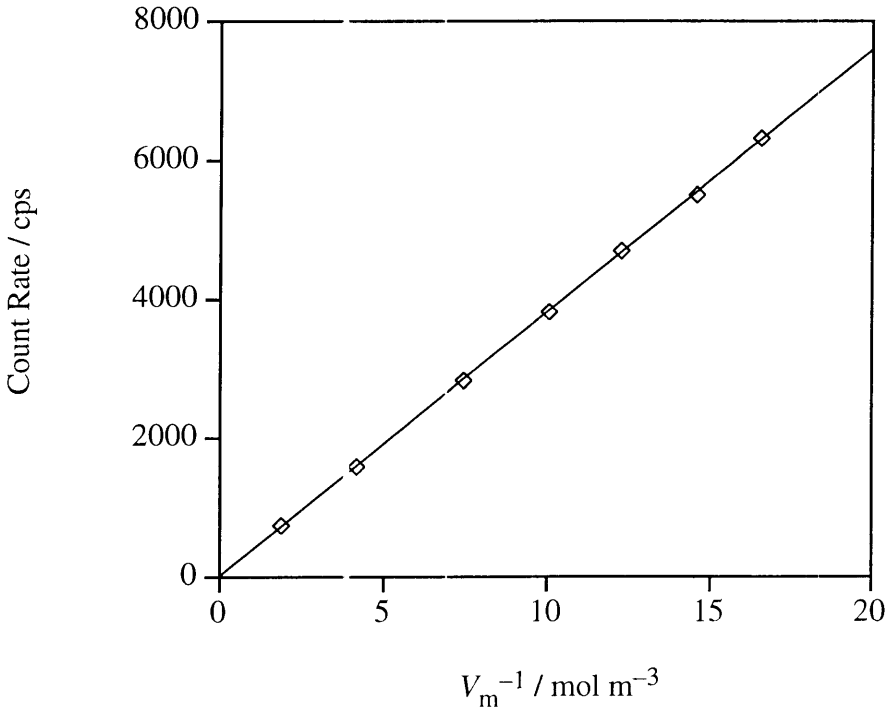

Figure 3.6 Depolarized count rates as a function of number density for carbon disulfide.

Table 3.4 Depolarization ratios, mean polarizabilities and polarizability anisotropies of carbon dioxide.

λ(nm)	$100\rho_0$	α	$\Delta\alpha$	Reference
632.8	4.01 ± 0.03	2.97 ± 0.03	2.33 ± 0.03[b]	Present work
632.8	3.99 ± 0.03[a]			Present work
632.8	4.03 ± 0.01	2.93	2.34	[23]
632.8	4.05 ± 0.02	2.933	2.350	[21]
647.1	4.04 ± 0.06	2.926	2.347	[20]
632.8	4.01 ± 0.04			[27]
632.8		2.93		[10]
632.8		2.936 ± 0.009		[29]
632.8		2.91		[30]
∞[c]		2.96	2.48	[19]
∞[c]		2.91	2.36	[15]
∞[c]		2.93	2.70	[18]

[a] Vibrational Raman lines excluded.

[b] Mean polarizabilities from the literature were used to calculate $\Delta\alpha$, see text.

[c] Calculated values.

Discussion

From Tables 3.4 and 3.5, it can be seen that the depolarization ratios for carbon dioxide and carbonyl sulfide obtained in the present research are in excellent agreement with the literature values. The ratio for carbonyl sulfide reported by Alms *et al.* [20], however, is too high. The mean polarizabilities obtained in the present research are higher than the available literature values. Since three other mean polarizabilities for carbon dioxide obtained from separate experiments are in agreement with one another, it is probable that the mean polarizabilities obtained in the present research for carbon dioxide and carbonyl sulfide are too high. The calculated mean polarizabilities of carbon dioxide are overestimates of the static polarizability of approximately 2.88 [18]. The

calculated values for carbonyl sulfide are underestimates. The values obtained by Russell and Spackman [19] for carbon dioxide are larger than those of Maroulis [15,17] and Spackman [18] due to the inclusion of zero-point vibrational averaging.

Table 3.5 Depolarization ratios, mean polarizabilities and polarizability anisotropies of carbonyl sulfide.

λ(nm)	$100\rho_0$	α	$\Delta\alpha$	Reference
632.8	3.90 ± 0.03	5.95 ± 0.03	4.54 ± 0.14[b]	Present work
632.8	3.88 ± 0.05[a]	5.79	4.53	[21]
647.1	3.99 ± 0.04	5.77	4.59	[20]
632.8	3.9 ± 0.1			[26]
632.8		5.76		[31]
632.8			4.53	[5]
632.8			4.49	[11]
∞			4.5 ± 0.2[d]	[13]
∞[c]		5.75	4.75	[19]
∞[c]		5.62	5.14	[18]

[a] Vibrational Raman lines excluded.

[b] Mean polarizabilities from the literature were used to calculate $\Delta\alpha$, see text.

[c] Calculated values.

[d] This value includes a correction for the vibrational polarizability [32], as quoted by Spackman [18].

The best estimates for the optical-frequency mean polarizabilities were taken as the means of the literature values: $\alpha(CO_2)$ = 2.93 ± 0.09 [9,10,20,21,33], α(OCS) = 5.775 ± 0.17 [20,21,31] and $\alpha(CS_2)$ = 9.54 ± 0.29 [20,21,31], with uncertainties of ± 1% assumed for carbon dioxide and ± 3% assumed for carbonyl sulfide and carbon disulfide. These values were used in the calculations of $\Delta\alpha$, $\alpha_{\parallel}$ and $\alpha_{\perp}$.

It will become apparent later in this thesis that the mean polarizabilities recorded with the present equipment either agree with the known literature values or are slightly

high, although usually by no more than ≈ 2%, and that the statistical uncertainty from a single determination of the mean polarizability is too small. The most probable source of uncertainty in the method of obtaining mean polarizabilities with the light scattering equipment is the mean polarizability of argon (Chapter 2), but this value is considered very reliable.

It must be emphasized that an accurate value of the mean polarizability is crucial to the calculation of the polarizability anisotropy, and other components of the polarizability if the symmetry permits. In the present research, the determination of the mean polarizability is of only secondary interest since, for the majority of molecules, it can be obtained accurately from other experiments. In the case of the present series of molecules, and carbon dioxide in particular, it would be inappropriate to use values of the mean polarizability which are in direct contradiction of what are usually highly accurate experimental results, especially when they are obtained from separate experiments.

The polarizability anisotropies obtained in the present work are in excellent agreement with the literature values given in Table 3.4. Of course, they depend on the value of the depolarization ratio used. The zero-frequency vibrationally averaged values of Russell and Spackman [19] are too large for carbon dioxide and carbonyl sulfide. The depolarization ratio and polarizability anisotropy obtained by Alms *et al.* [20] for carbonyl sulfide are too large. The zero-frequency value for carbonyl sulfide from a Stark Effect measurement by Scharpen *et al.* [13], with an appropriate vibrational polarizability anisotropy correction [18], is slightly larger than the present polarizability anisotropy. The optical-frequency value for carbonyl sulfide from the refractivity data of Elliot and Ward [11] is too small. The optical-frequency polarizability anisotropy obtained by Kling and Hüttner [5], using Cotton-Mouton and microwave Zeeman effect studies, is in excellent agreement with the present value. The polarizability components for carbon dioxide were found to be $\alpha_{\parallel} = 4.48 \pm 0.04$ and $\alpha_{\perp} = 2.15 \pm 0.03$, and the polarizability components for carbonyl sulfide were found to be $\alpha_{\parallel} = 8.80 \pm 0.23$ and $\alpha_{\perp} = 4.26 \pm 0.18$.

A summary of the relevant electric properties of carbon disulfide is given in Table 3.6. The ratio of $100\rho_0 = 7.41 \pm 0.03$ for carbon disulfide (see the following section) compares poorly with the literature values of Bogaard *et al.* [21] and Baas and van den Hout [26], but agrees well with Alms *et al.* [20]. Since these were single-pressure measurements, comparison with the present result is probably not valid, although it is possibly a reflection of the quality of the value obtained by Alms *et al.*

Table 3.6 Depolarization ratios, mean polarizabilities and polarizability anisotropies of carbon disulfide.

λ(nm)	$100\rho_0$	α	$\Delta\alpha$	Reference
632.8	7.41 ± 0.03^a	10.17 ± 0.03	10.71 ± 0.32^b	Present work
632.8	7.18 ± 0.07	9.65	10.53	[21]
647.1	7.41 ± 0.07	9.67	10.74	[20]
632.8	7.3 ± 0.2			[26]
∞^c		9.41	10.27	[19]
∞^c		9.14	9.33	[17]
∞^c		9.03	10.36	[18]

a Vibrational Raman lines included.

b Mean polarizabilities from the literature were used to calculate $\Delta\alpha$, see text.

c Calculated values.

Only one mean polarizability was recorded for carbon disulfide, giving α = 10.17 ± 0.03, which is too large when compared with values obtained from other experiments, and has a statistical uncertainty which is definitely an underestimate. The static vibrationally averaged value reported by Russell and Spackman [19] is small for carbon disulfide. The SCF value reported by Maroulis [17] is too small, but inclusion of electron correlation and vibrational averaging would increase this value. The value of $\Delta\alpha$ for carbon disulfide reported by Bogaard *et al.* [21] is too small since the depolarization ratio is smaller than the present ratio. The polarizability components for carbon disulfide were determined to be $\alpha_\parallel = 16.78 \pm 0.45$ and $\alpha_\perp = 6.07 \pm 0.31$.

Coonan [6] has reported studies of the temperature dependence of the Cotton-Mouton effects for this series of molecules which, using equation 1.36, enables a determination of the quadrupole moment. There is a negligible discrepancy between the present polarizability anisotropies and those used by Coonan for carbon dioxide and carbonyl sulfide. For carbon disulfide, however, the present polarizability anisotropy is approximately 1.7% higher. Recalculation of the results using the present polarizability anisotropy gives: $\Delta\chi = (-30.2 \pm 1.0) \times 10^{-29}$ J T^{-2} and $\Theta = (12.7 \pm 1.9) \times 10^{-40}$ C m^2 where $\Delta\chi$ and Θ are 6% and 8% lower, respectively, than the values given by Coonan. Watson [7] has reported studies of the temperature dependence of the field-gradient birefringence effects for carbon dioxide and carbon disulfide. A reanalysis of the carbon disulfide results using the present polarizability anisotropy gives $\Theta = (11.3 \pm 0.6) \times 10^{-40}$ C m^2 which is 1.7% lower than the original value, but within the experimental uncertainty.

Pressure dependence of the depolarization ratio of carbon disulfide

Single-pressure measurement of the depolarization ratio has been a standard method in light scattering for decades. Bridge and Buckingham [23] investigated carbon dioxide and chloromethane up to ≈ 100 kPa and found the pressure dependence to be negligible. Bogaard *et al.* [21] observed a small change (< 1%) in the value of ρ_0 for allene, bromomethane, chloromethane and isobutane for pressures up to ≈ 100 kPa. Alms, Burnham and Flygare [20] used the depolarization ratio of carbon disulfide to check the linearity of their photon counting system. They observed negligible pressure dependence for the gases studied, including carbon disulfide. Hesling [27] did not observe pressure dependences of the ratios for the species he studied. Overall, it was assumed that ratios recorded at pressures below ≈ 100 kPa for gases, and 1/2 to 2/3 of the equilibrium vapour pressure for vapours, would result effectively in free-molecule ratios. This is, in general, an excellent assumption, and one that has been applied in the present research.

The density dependence of the depolarization ratio can be expressed as a virial expansion in the molar volume, V_m [34]

$$\rho = \rho_0 + \frac{B_\rho}{V_m} + \frac{C_\rho}{V_m^2} + \ldots \tag{3.1}$$

where ρ_0 is the zero-density depolarization ratio; B_ρ and C_ρ are the light scattering second and third virial coefficients which describe contributions from pairs and triplets of molecules to the depolarization ratio.

The depolarization ratio can be expressed as an interaction of the differential polarizabilities for a pair of molecules [35]

$$\rho = \frac{\left\langle \pi_{zx}^{(1)} \pi_{zx}^{(1)} \right\rangle + \left\langle \pi_{zx}^{(1)} \pi_{zx}^{(2)} \right\rangle}{\left\langle \pi_{xx}^{(1)} \pi_{xx}^{(1)} \right\rangle + \left\langle \pi_{xx}^{(1)} \pi_{xx}^{(2)} \cos\chi_{12} \right\rangle} \tag{3.2}$$

where $\pi_{\alpha\sigma}^{(p)}$ is the differential polarizability of a molecule p in space-fixed axes (x, y, z) and, χ_{pq} is the phase difference in the light scattered by molecules p and q. The brackets indicate averaging over configurations of the sample. The differential polarizability is

$$\pi_{\alpha\sigma}^{(p)} = \alpha_{\alpha\sigma}^{(p)} + \alpha_{\alpha\delta}^{(p)} T_{\delta\varepsilon} \alpha_{\varepsilon\sigma}^{(p)} + \alpha_{\alpha\delta}^{(p)} T_{\delta\gamma} \alpha_{\gamma\beta}^{(q)} T_{\beta\varepsilon} \alpha_{\varepsilon\sigma}^{(p)} + \ldots \tag{3.3}$$

where $T_{\alpha\beta}$ is the second order T-tensor [36]. This equation is limited to dipole-dipole interactions, although field-gradient effects and induced quadrupole moments can be included [37].

Following tensor manipulations [35,37], substituting equation 3.3 into equation 3.2, and expressing ρ as a virial expansion, as in equation 3.1, gives the result

$$B_\rho = \rho_0 \left(1 - \frac{4}{3}\rho_0\right)(2B + \varphi) \tag{3.4}$$

where φ is the summation of angular correlation, dipole-dipole, field gradient and induced quadrupole moment effects and B is the normal density second virial coefficient.

From equation 3.1, assuming only pair-wise interactions are significant, a plot of the depolarization ratio as a function of the number density gives the zero density depolarization ratio ρ_0 as the intercept and B_ρ as the gradient. Therefore, from equation

3.4, a knowledge of B allows an estimation of the contribution of φ to the light scattering second virial coefficient B_ρ.

Least-squares analysis of the data in Table 3.2 gives an intercept of $100\rho_0 = 7.402 \pm 0.013$, but since the correlation was only 95%, the zero density ratio will be quoted as $100\rho_0 = 7.41 \pm 0.03$. It is assumed that the depolarization ratios at higher gas densities are slightly overestimated due to higher order interactions which skew the zero-density ratio to a lower value. The least-squares analysis gave a gradient of $B_\rho = (-2.63 \pm 0.14) \times 10^{-4}\ m^3\ mol^{-1}$. Equation 3.4 can then be rearranged to solve for φ giving,

$$\varphi = -\frac{B_\rho}{\rho_0\left(1-\frac{4}{3}\rho_0\right)} - 2B \tag{3.5}$$

Therefore, an estimate of the angular correlations etc. is $\varphi = (-2.21 \pm 0.22) \times 10^{-3}\ m^3\ mol^{-1}$ using a smoothed value of B from the literature [25] (B(290K) = $(-862 \pm 30) \times 10^{-6}\ m^3\ mol^{-1}$). It is noted that the virial coefficients given in the literature are subject to large uncertainties. For carbon disulfide, it is clear that the contributions from angular correlation, field gradient, and induced quadrupole moment effects to B_ρ are $\approx$ 56% of the total contribution to the observed light scattering second virial cofficient.

Since the density dependence has a negative slope, the pair-wise interaction at higher densities results in a decrease in the anisotropy and, from equation 1.10, this results in smaller depolarization ratios. It is likely that the main source of interaction for carbon disulfide is a quadrupole-quadrupole interaction, which has a greater probability of occurrence at higher densities, and this explains the negative value of B_ρ. This is supported by research on carbon dioxide by Dayan *et al.* [28], in which a negative contribution to B_ρ was observed and attributed to quadrupolar angular correlation. Also of interest is that the value of B_ρ for carbon disulfide is 30 times larger than the values reported for carbon dioxide by Dayan *et al.* and Couling and Graham [38].

Conclusions

The depolarization ratio for carbon dioxide was found to be in excellent agreement with the literature values, and was used to check the equipment. The depolarization ratio for carbonyl sulfide was found to agree with the result reported by Bogaard *et al.* [21], and not the value reported by Alms *et al.* [20]. The depolarization ratio for carbon disulfide was found to have a linear density dependence. The free-molecule depolarization ratio was determined to be $100\rho_0 = 7.41 \pm 0.03$, where contributions from vibrational Raman lines were assumed to be negligible. A value for the light scattering second virial coefficient was calculated and the contribution from angular correlations etc. was determined. A density dependence of the depolarization ratio of carbon dioxide was not found. The mean polarizabilities for carbon dioxide and carbonyl sulfide determined with the present equipment were found to be overestimates, but the method was considered unreliable for determining the mean polarizability of carbon disulfide. Mean polarizabilities obtained from the literature, and the present depolarization ratios, were combined to calculate the polarizability anisotropy and polarizability components for each molecule.

References

1. Buckingham, A.D., Bogaard, M.P., Dunmur, D.A., Hobbs, C.P. and Orr, B.J., *Trans. Faraday Soc.*, **66**, 1548 (1970).
2. Blanch, E.W. and Ritchie, G.L.D., unpublished results.
3. Bogaard, M.P., Buckingham, A.D. and Ritchie, G.L.D., *Mol. Phys.*, **18**, 575 (1970).
4. Gentle, I.R., Laver, D.R. and Ritchie, G.L.D., *J. Phys. Chem.*, **93**, 3035 (1989).
5. Kling, H. and Hüttner, W., *Chem. Phys.*, **90**, 207 (1984).
6. Coonan, M.H., *"Temperature dependence of the Cotton-Mouton effect in gases"*, Ph.D. Thesis, University of New England, (1995).
7. Watson, J.N., *"The measurement of field-gradient induced birefringence in gases"*, Ph.D. Thesis, University of New England, (1994).
8. Buckingham, A.D. and Disch, R.L., *Proc. Roy. Soc. A*, **273**, 275 (1963).
9. Hohm, U., *Chem. Phys.*, **179**, 533 (1994).
10. Hohm, U., *Mol. Phys.*, **81**, 157 (1994).
11. Elliott, D.S. and Ward, J.F., *Phys. Rev. Lett.*, **46**, 317 (1981).
12. Scharpen, L.H., Muenter, J.S. and Laurie, V.W., *J. Chem. Phys.*, **46**, 2431 (1967).
13. Scharpen, L.H., Muenter, J.S. and Laurie, V.W., *J. Chem. Phys.*, **53**, 2513 (1970).
14. Tanaka, K. and Tanaka, T., *J. Chem. Phys.*, **82**, 2835 (1985).
15. Maroulis, G. and Thakkar, A.J., *J. Chem. Phys.*, **93**, 4164 (1990).
16. de Brouckère, G., Feller, D. and Berthier, G., *J. Phys. B: At. Mol. Phys.*, **20**, (1987).
17. Maroulis, G., *Chem. Phys. Lett.*, **199**, 250 (1992).
18. Spackman, M.A., *J. Phys. Chem.*, **93**, 7594 (1989).
19. Russell, A.J. and Spackman, M.A., unpublished results.
20. Alms, G.R., Burnham, A.K and Flygare, W.H., *J. Chem. Phys.*, **63**, 3321 (1975).

21. Bogaard, M.P., Buckingham A.D., Pierens, R.K. and White, A.H., *J. Chem. Soc., Faraday Trans. 1*, **74**, 3008 (1978).

22. Perrin, D.D., Armarego, W.L.F. and Perrin, D.R., *"Purification of laboratory chemicals"*, 2nd Edition (Pergamon, Oxford, 1980).

23. Bridge, N.J. and Buckingham, A.D., *Proc. Roy. Soc. A*, **295**, 334 (1966).

24. Pitzer, K.S., *J. Am. Chem. Soc.*, **77**, 3427 (1955).

25. Dymond, J.H. and Smith, E.B., *"The virial coefficients of pure gases and mixtures"*, (Oxford University Press, Oxford, 1980).

26. Baas, F. and van den Hout, K.D., *Physica*, **95**, 597 (1979).

27. Hesling, M.R., *"Measurements of Rayleigh depolarization ratios of gases and vapours."*, Ph.D. Thesis, University of New England, (1990).

28. Dayan, E., Dunmur, D.A. and Manterfield, M.R., *J. Chem. Soc., Faraday Trans. 2*, **76**, 309 (1980).

29. St Arnaud, J.M. and Bose, T.K., *J. Chem. Phys.*, **68**, 2129 (1978).

30. Burns, R.C., Graham, C. and Weller, A.R.M., *Mol. Phys.*, **59**, 41 (1986).

31. Kumar, A. and Meath, W.J., *Can. J. Phys.*, **63**, 417 (1985).

32. Bishop, D.M. and Cheung, L.M., *J. Phys. Chem.*, **11**, 119 (1982).

33. St-Arnaud, J.M. and Bose, T.K., *J. Chem. Phys.*, **71**, 4951 (1979).

34. Buckingham, A.D. and Stephen, M.J., *Trans. Faraday Soc.*, **53**, 884 (1957).

35. Graham, C., *Mol. Phys.*, **77**, 291 (1992).

36. Buckingham, A.D., *Adv. Chem. Phys.*, **12**, 107 (1967).

37. Couling, V.W. and Graham, C., *Mol. Phys.*, **79**, 859 (1993).

38. Couling, V.W. and Graham, C., *Mol. Phys.*, **82**, 235 (1994).

Chapter Four

Boron trihalides

Introduction

There is much interest in the electric and magnetic properties of the boron trihalides due to their relatively simple, highly symmetrical structures. Studies of the electric and magnetic properties of these species have been few in number, due to their high reactivity and corrosive nature. The boron trihalides react vigorously with water producing boric acid and hydrogen halides, and in the case of boron trifluoride BF_3OH may be formed [1]. For boron trifluoride, the hydrofluoric acid formed will devitrify glass, especially at high temperatures. The boron trihalides also tend to harden Viton o-rings and seals. Solution-phase Kerr effect measurements have been recorded for the series by Armstrong *et al.* [2]. Novick [3] has reported estimates of the molecular quadrupole moment, Θ, and the parallel component of the polarizability, $\alpha_{\parallel}$, for boron trifluoride. There is also an unpublished study of the field-gradient induced birefringence of boron trifluoride by Graham, Imrie and Raab [4]. Other physical studies have focused on the determination of the geometries of the molecules using infrared analysis [5] and electron diffraction [6-9].

Computational studies of the complete series are few, and have concentrated on reactivities, complexation, dimer formation and catalysis. Tossell and Lazzeretti [10] have reported calculations of the field-gradients and NMR shielding tensors. Branchadell and Oliva [11] used the SCF and MP2 levels of theory with small basis sets to calculate

geometries, energies and populations of the states for this series of molecules. The research, however, concentrated on the Lewis acidity scale of this series. Recently, Fowler *et al.* [12] have reported CHF and anisotropic bond polarizability model calculations of the multipole polarizabilities and dispersion coefficients for boron trifluoride. Ángyán *et al.* [13] have reported polarizabilities calculated by partitioning the molecular charge density into atomic domains.

Overall, there is a distinct lack of reliable experimental and theoretical information available for the electric properties of this series of molecules. The depolarization ratios given in this chapter are the first reported values of these quantities for the boron trihalides. Mean polarizabilities are determined for boron trifluoride and boron trichloride, and the polarizability anisotropies and polarizability components are calculated for boron trifluoride, boron trichloride and boron tribromide. Ab initio calculations of the electric properties are included.

Experimental details

Boron trifluoride is a gas at room temperature with a boiling point of −100 °C. Boron trichloride is a volatile liquid with a boiling point of 12.5 °C. Boron tribromide is also a liquid with a boiling point of 90 °C, which is low enough to be studied with the present apparatus. Boron triiodide could not be studied because its melting point of 43 °C is too high to obtain a sufficient vapour pressure within the light scattering cell, and this is compounded by the high boiling point of 210 °C. Boron trifluoride was obtained from the Aldrich Chemical Company (> 99.5%), and was used without further purification. Boron trichloride was obtained from Hopkin and Williams Ltd (purity unspecified) and boron tribromide was obtained from BDH Ltd (> 99%). The liquids were subjected to two freeze-pump-thaw cycles, which included a vacuum distillation, before use. Gas-chromatographic analysis was attempted for boron trichloride to determine the purity, but breakdown products in the column precluded a successful determination. The purity was assumed to be at least 98% because, after the freeze-pump-thaw cycles and vacuum distillation, the liquid was clear and free of any visible acidic residues. The boron

tribromide sample contained a reddish-orange colour due to the presence of elemental bromine [14], and this was removed on vacuum distillation.

The depolarization ratios for boron trifluoride and boron trichloride are given in Table 4.1. The values were obtained at 25 °C and ≈ 100 kPa using Version 2 of the equipment, and with inclusion and exclusion of the vibrational Raman lines. For boron trifluoride, typical depolarized and polarized counts were approximately 46 and 11 400 cps, with background counts of 4 and 14 cps, respectively. Excellent signal strength was obtained for boron trichloride; the unfiltered depolarized and polarized counts were approximately 1 580 and 162 000 cps, with background counts of 8 and 26 cps, respectively.

Table 4.1 Depolarization ratios for boron trifluoride, boron trichloride and boron tribromide.

$100\rho_0$				
BF_3		BCl_3		BBr_3
0.379 ± 0.011	0.363 ± 0.011[a]	0.971 ± 0.003	0.995 ± 0.002[a]	1.210 ± 0.006
0.366 ± 0.007	0.363 ± 0.011[a]	0.985 ± 0.002	0.982 ± 0.002[a]	1.227 ± 0.005
0.380 ± 0.008	0.370 ± 0.013[a]	0.971 ± 0.002	0.995 ± 0.002[a]	1.230 ± 0.005
0.375 ± 0.009	0.353 ± 0.012[a]	0.983 ± 0.002	0.983 ± 0.002[a]	1.227 ± 0.005
0.381 ± 0.015	0.383 ± 0.012[a]	0.978 ± 0.002	0.992 ± 0.003[a]	1.211 ± 0.005
0.366 ± 0.010	0.347 ± 0.012[a]	0.975 ± 0.002		

[a] Vibrational Raman lines excluded.

Table 4.1 also includes depolarization ratios for boron tribromide. The vibrational Raman lines were not excluded because it was evident from the results for boron trichloride that their contribution to the depolarization ratio would be negligible and, due to the corrosive nature of this compound, it was thought prudent to minimize the length of time the compound was present in the plumbing system. Five ratios were recorded at 97.5 °C and ≈ 30 kPa with Version 2 of the equipment. Typical depolarized

and polarized counts were 794 and 64 100 cps, with background counts of 18 and 27 cps, respectively. Integration times for the depolarized and polarized components were 400 and 200 s for boron trifluoride, 300 and 150 s for boron trichloride, and 200 and 100 s for boron tribromide.

One mean polarizability was recorded for both boron trifluoride and boron trichloride with the vibrational Raman lines excluded. It was not possible to record a mean polarizability for boron tribromide due to the low vapour pressure available. The density second virial coefficients for boron trichloride were calculated using the method of Pitzer [15], giving $B(290\ \mathrm{K}) = -931.6 \times 10^{-6}\ \mathrm{m^3\ mol^{-1}}$ and $B(300\ \mathrm{K}) = -860.1 \times 10^{-6}\ \mathrm{m^3\ mol^{-1}}$. Virial coefficients for boron trifluoride and boron tribromide were obtained from the literature [16].

Discussion

The depolarization ratios, mean polarizabilities and polarizability anisotropies for the three molecules are given in Table 4.2. There are no known literature values for the depolarization ratios of these compounds. The mean polarizabilities for boron trifluoride and boron trichloride obtained in the present research were given uncertainties of ± 5%, since only one mean polarizability was determined for each molecule. From Table 4.2 it is clear that the agreement with the literature values of the mean polarizability is poor. For boron trifluoride, the present mean polarizability is 4.6% smaller than the values derived from refractive indices interpolated to 632.8 nm and measurements of the relative permittivity. This is an exception to the general observation in the present work that mean polarizabilities obtained using the Rayleigh light scattering equipment are usually slightly larger than values derived from refractive indices. For boron trichloride, the present mean polarizability is 6.6% larger than the value derived from refractive indices and 9.6% smaller than from measurements of the relative permittivity. The mean polarizabilities derived from measurements of the relative permittivity have vibrational polarizability corrections of $\alpha_{vib} = 0.98$ for boron trifluoride and $\alpha_{vib} = 0.41$ for boron trichloride [17], but are not expected to be as accurate as the values obtained from refractive indices. The polarizability anisotropies were calculated using the mean

polarizabilities interpolated to 632.8 nm from the gas- and liquid-phase refractive indices of Lowery [18] and Watson and Ramaswamy [19], with assumed uncertainties of ± 3%.

Table 4.2 Depolarization ratios, mean polarizabilities and polarizability anisotropies of boron trifluoride, boron trichloride and boron tribromide.

Molecule	λ(nm)	$100\rho_0$	α	$\Delta\alpha$	Reference
BF_3	632.8	0.375 ± 0.007	2.59 ± 0.13		Present work
	632.8	0.363 ± 0.013[a]		−0.63 ± 0.03	Present work
	632.8		2.71		[19]
	∞		2.70		[20]
BCl_3	632.8	0.997 ± 0.006	9.77 ± 0.49		Present work
	632.8	0.989 ± 0.007[a]		−3.55 ± 0.11	Present work
	632.8		9.16		[18]
	∞		10.13		[20]
BBr_3	632.8	1.22 ± 0.01		−5.65 ± 0.18	Present work
	632.8		13.1 ± 0.4		[18]

[a] Vibrational Raman lines excluded.

An unpublished single-temperature measurement of the molar field-gradient birefringence constant of boron trifluoride was recorded by Graham, Imrie and Raab [4]. This study assumed a negligible contribution from the quadrupole hyperpolarizability, B, as given in equation 1.38. A value for $\Delta\alpha$ was unknown prior to the present study and the product $\Delta\alpha\Theta = (-7.93 \pm 0.08) \times 10^{-30}\ C^2\ m^4\ V^{-1}$ was reported. Combining this result with the polarizability of $\Delta\alpha = -0.63 \pm 0.03$ obtained in the present research, gives a quadrupole moment for boron trifluoride of $\Theta = (12.6 \pm 0.6) \times 10^{-40}\ C\ m^2$.

Novick [3] has estimated the quadrupole moment of boron trifluoride from Stark effect measurements of the dipole moments of van der Waals complexes. By considering the contributions from the appropriate electrostatic interactions to the induced moments of $ArBF_3$ and BF_3CO, a set of simultaneous equations was solved to give a quadrupole

moment for boron trifluoride of Θ = 11.2 x 10^{-40} C m^2. This self-consistent approach to the calculation gives good agreement with the present value. Novick notes that the multipole expansion, as given by equation 1.1, is only slowly convergent for molecules at relatively close distances, such as is found in van der Waals complexes. Contributions from the dipole moment induced by an electric field-gradient, $E'_{\beta\gamma}$, which contributes $+A_{\alpha,\beta\gamma}E'_{\beta\gamma}/3$ to equation 1.1 have been ignored but may be significant. Novick does not estimate an uncertainty for the quadrupole moment, and it is probable that neglecting higher contributions from the multipole expansion will give a quadrupole moment that is too small. The results give support to the assumption that electrostatic interactions are the main contribution to the dipole moments of van der Waals complexes.

The polarizability components were calculated from the depolarization ratios and mean polarizabilities and are given in Table 4.3. The values given in parentheses are estimates of the free-molecule polarizability components from the solution-phase Kerr effect work of Armstrong *et al.* [2], and are in reasonably good agreement with the present results. Armstrong could not determine the components for boron trifluoride with either cyclohexane or dioxane as the solvent.

Novick [3] reported a value of the parallel component of the polarizability for boron trifluoride of $\alpha_{\parallel}$ = 5.43. This value includes a contribution from the vibrational polarizability, $\alpha_{\parallel}^{vib}$. An estimate of this contribution can be obtained from the work of Bishop and Cheung [17], giving $\alpha_{\parallel}^{vib}$ = 0.765. Therefore, the electronic parallel component of the polarizability is $\alpha_{\parallel}^{elec}$ = 4.66. In comparison with the component obtained in the present research, the value given by Novick is too large. As noted above, there are inherent approximations in the method used by Novick.

Studies of the gas-phase Kerr effect of the boron trihalides would provide some interesting results. From equation 1.31, the Kerr second hyperpolarizability, γ^K, and the static polarizability anisotropy, $\Delta\alpha^0$, could be determined. The study of the gas-phase Kerr effect would be challenging, since the boron trihalides are extremely corrosive and would be subjected to high temperatures and large AC and DC voltages.

Table 4.3 Polarizability components for boron trifluoride, boron trichloride and boron tribromide.[a]

Molecule	$\alpha_{\parallel}$	$\alpha_{\perp}$
BF_3	2.29 ± 0.09	2.92 ± 0.08
BCl_3	6.79 ± 0.30	10.34 ± 0.27
	(6.59)	(10.0)
BBr_3	9.33 ± 0.44	14.98 ± 0.41
	(8.88)	(14.5)

[a] Values in parentheses are from solution-phase Kerr effect measurements [2].

From equation 1.35, it is clear that studies of the gas-phase Cotton-Mouton effect would determine the magnetic hyperpolarizability anisotropy, $\Delta\eta$, and the magnetizability anisotropy, $\Delta\chi$, and some work has already been done on boron trichloride [21]. The determination of the magnetizability anisotropy would be another route to the calculation of the quadrupole moment using equation 1.36. The other principle method of calculating the magnetizability anisotropy is by means of the microwave Zeeman effect, but this method requires the presence of a permanent dipole moment [22]. As far as is known, values of the magnetizability anisotropies and molecular g values of the boron trihalides have not been reported, but it could be possible to study the van der Waals complexes $ArBF_3$ and BF_3CO since they are dipolar species.

Theoretical calculations

The present computational study was undertaken to calculate the electric properties of the boron trihalides with consistent geometries and basis sets. Due to the presence of the bromine and iodine atoms, a relatively small basis set was required. Research on such a basis set was reported by Dougherty and Spackman [23], where the HUZ-SV basis set was augmented with s and d polarization functions, giving the HUZ-SV(+sd) basis set. The geometries used in the calculations were taken from the literature, giving r_g(B–F) = 0.1313 nm, r_g(B–Cl) = 0.1742 nm, r_g(B–Br) = 0.1893 nm and

r_g(B–I) = 0.2118 nm [6], where ar r_g structure is averaged over thermal vibrations.

The calculations were per ormed with the CADPAC program using the CHF method, except for the MP2 corr ctions for boron trichloride and boron tribromide, which were calculated using the finite-field method with the CADPAC and GAMESS programs, respectively. Zero-frequency and optical-frequency values for the polarizability components are given in Tables 4.4 and 4.5. A summary of frequency dependent polarizabilities is given in Appendix I. Recent calculations by Kellö and Sadlej on the hydrogen halides [24] and cyanogen halides [25] have indicated that the relativistic contribution to dipole polarizabil ties is small, positive and non-negligible only for molecules containing iodine; relativ stic effects were ignored in the present study.

From the tables, the polari zability components increase along the series boron trifluoride, boron trichloride, bc ron tribromide, and boron triiodide. The MP2 calculations of the mean polarizability at 632.8 nm are too large by 8% and 0.6% for boron trifluoride and boron tribrom de, and too small by 1.5% for boron trichloride. The calculated polarizability anisotropies are too large by 11% and 2.3% for boron trifluoride and boron trichloride, and too small by 0.5% for boron tribromide. Overall, this is excellent agreement considering the difficulty in calculating this property exactly. The polarizability components are too small for boron trifluoride and boron trichloride, and too large for boron tribromide.

Fowler *et al.* [12] reported polarizability components of $\alpha_{\parallel}$ = 2.259 and $\alpha_{\perp}$ = 3.165 for boron trifluoride from CHF calculations using Sadlej substrates with added polarization functions, and these static values are too large. Recent work reported by Ángyán *et al.* [13] calculated the polarizabilities at the CHF level of theory by partitioning the molecular charge density into atomic domains, and basis sets derived from the 6-311G substrate were used in the calculations. The polarizability components calculated with this method were too small, however, agreement may be improved by the use of larger basis sets and the inclusion of electron correlation corrections.

Table 4.4 Zero-frequency polarizability components for the boron trihalides using the HUZ-SV(+sd) basis set.

	BF_3		BCl_3		BBr_3		BI_3	
	SCF	MP2	SCF	MP2	SCF	MP2	SCF	MP2
$\alpha_\perp$	2.271	2.714	8.885	10.066	12.977	14.705	20.527	23.178
$\alpha_\parallel$	1.748	2.040	6.031	6.521	8.572	9.267	13.137	14.043
α	2.101	2.489	7.934	8.384	11.509	12.982	18.064	20.133
$\Delta\alpha$	−0.510	−0.674	−2.853	−3.545	−4.405	−5.439	−7.389	−9.136

Table 4.5 Polarizability components for the boron trihalides at 632.8 nm using the HUZ-SV(+sd) basis set.

	BF_3		BCl_3		BBr_3		BI_3	
	SCF	MP2	SCF	MP2	SCF	MP2	SCF	MP2
$\alpha_\perp$	2.288	2.731	9.059	10.240	13.328	15.056	21.350	24.001
$\alpha_\parallel$	1.773	2.051	6.116	6.606	8.733	9.428	13.473	14.379
α	2.116	2.504	8.078	9.029	11.796	13.180	18.725	20.794
$\Delta\alpha$	−0.515	−0.680	−2.943	−3.634	−4.595	−5.628	−7.878	−9.623

Polarizabilities for boron trifluoride and boron trichloride are given in Appendix I at the SCF and MP2 levels of theory for both the HUZ-SV(+sd) and 6-31G(+pd) basis sets. A description of the 6-31G(+pd) basis set is given in Appendix I. The 6-31G(+pd) basis set calculations were included to provide a benchmark for the HUZ-SV(+sd) basis set. From Tables A1 and A2, it is evident that the MP2 polarizabilities for 632.8 nm calculated using the 6-31G(+pd) basis set, when compared with experiment, are as accurate as the HUZ-SV(+sd) results. The 6-31G(+pd) basis set is not defined for

bromine or iodine, so the HUZ-SV(+sd) basis set should provide excellent estimates of the polarizability components for boron tribromide and boron triiodide.

Quadrupole moments were also calculated from energy derivatives using the HUZI-SV(+sd+sp) basis set at the MP2 level of theory. The quadrupole moments were found to be Θ = 14.4 x 10^{-40} C m^2 for boron trifluoride, Θ = 5.30 x 10^{-40} C m^2 for boron trichloride, and Θ = 0.17 x 10^{-40} C m^2 for boron tribromide. The value calculated for boron trifluoride is in reasonable agreement with the experimental value of Θ = 12.6 x 10^{-40} C m^2. The agreement between these results indicates that the single temperature measurement of the molar field-gradient birefringence constant, ${}_mQ$, given in the unpublished study by Graham, Imrie and Raab [4], which assumed a negligible contribution from the quadrupole hyperpolarizability, was a reasonable approximation. The contribution from the quadrupole hyperpolarizability is probably less than 10% of the value of ${}_mQ$ at ≈ 300K. This is contrary to temperature dependent measurements of the molar field-gradient birefringence constant of other small, highly symmetrical molecules reported by Watson [26]. For ethane and cyclopropane, the contributions to ${}_mQ$ from the quadrupole hyperpolarizabilities was found to be 37% and 52%, respectively.

The sign and magnitudes of the quadrupole moments can be rationalized by separating the nuclear and electronic contributions to the quadrupole moments [27]. For species with C_{3v} or higher symmetry, the quadrupole moment can be expressed as

$$\Theta = e\left[\sum_n Z_n \left(z_n^2 - x_n^2\right)\right] - e\left[\left\langle z^2\right\rangle - \left\langle x^2\right\rangle\right] \qquad (4.1)$$

where e is the protonic charge, Z_n is the atomic number of the n-th nucleus and $\left\langle z^2\right\rangle - \left\langle x^2\right\rangle$ is the anisotropy in the second moment of the electronic charge distribution.

For boron trifluoride, the electronegative fluorine atoms withdraw the electronic charge density to the periphery of the molecule leaving an electron deficient central boron atom. Consequently, the term $\left\langle z^2\right\rangle - \left\langle x^2\right\rangle$ is more negative than if there were no interactions between the atoms, which results in a positively signed quadrupole moment.

The magnitude of the quadrupole moment decreases as the size of the halogen

increases. The chlorine and bromine atoms are less electronegative than the fluorine atom, therefore the withdrawal of the electronic charge away from the central atom is less. The contribution from the term $\langle z^2 \rangle - \langle x^2 \rangle$ is reduced so that, although the quadrupole moments are positive, the magnitudes decrease.

Intuitively, this withdrawal of electronic charge density to give an electropositive center would imply a Lewis acidity scale corresponding to the size of the quadrupole moments, i.e. $BF_3 > BCl_3 > BBr_3 > BI_3$, however, the experimentally determined order of the acid strength of the boron trihalides is the reverse. Branchadell and Oliva [11] suggest that this ordering is because, although there is a loss of σ orbital population, it is partially compensated by an increase in π donation back to the boron atom. Therefore, acid strength increases as the double-bond character of the boron-halogen bond decreases, as occurs along the series BF_3, BCl_3, BBr_3, and BI_3. The partial pyramidalization required of the boron trihalides to form Lewis acid complexes must also be considered because the energy required for pyramidalization will decrease as the double-bond character decreases. Of course, binding energies of Lewis acid complexes are also dependent on other factors, such as the electrostatic and dative components of the BX_3–ligand interaction, and the type of interaction will depend on the electronic structure of the ligand [28,29], and in some cases steric effects may also be significant.

Conclusions

The depolarization ratios of the boron trihalides were reported for the first time. Mean polarizabilities were determined for boron trifluoride and boron trichloride and were found to be in reasonable agreement with the literature data. Excellent agreement was found between the polarizability anisotropies and polarizability components determined experimentally and computationally. The quadrupole moment for boron trifluoride was determined from an unpublished study of the molar field-gradient birefringence constant by Graham, Imrie and Raab. This value is in good agreement with quadrupole moments calculated in the present work. It is probable that the quadrupole hyperpolarizability contribution to the molar field-gradient birefringence constant of boron trifluoride is less than 10% of the value of ${}_{\mathrm{m}}Q$ at ≈ 300 K.

References

1. Finch, A. and Gardner, P.J., Thermochemistry of boron compounds. In *"Progress in boron chemistry"*, Brotherton, R.J. and Steinberg, H. (Ed.), (Pergamon, Oxford, 1970).
2. Armstrong, R.S., Aroney, M.J , Hector, A. and Le Fèvre, R.J.W., *J. Chem. Soc. B*, 1203 (1968).
3. Novick, S.E., *J. Phys. Chem.*, **90**, 3871 (1986).
4. Graham, C., Imrie, D.A. and Raab, R.E., unpublished results.
5. Ginn, S.G.W., Kenney, J.K. and Overend, J., *J. Chem. Phys.*, **48**, 1571 (1968).
6. Kakubari, H., Konaka, S. and Kimura, M., *Bull. Chem. Soc. Japan*, **47**, 2337 (1974).
7. Konaka, S., Murata, Y., Kuchitsu, K. and Morino, Y., *Bull. Chem. Soc. Japan*, **39**, 1134 (1966).
8. Konaka, S., Ito, T. and Morino, Y., *Bull. Chem. Soc. Japan*, **39**, 1146 (1966).
9. Kuchitsu, K. and Konaka, S., *J Chem. Phys.*, **45**, 4342 (1966).
10. Tossell, J.A. and Lazzeretti, P , *J. Phys. B: At. Mol. Phys.*, **19**, 3217 (1986).
11. Branchadell, V. and Oliva, A., *J. Mol. Struct. (Theochem)*, **82**, 75 (1991).
12. Fowler, P.W., Kelly, H.M. and Vaidehi, N., *Mol. Phys.*, **82**, 211 (1994).
13. Ángyán, J.G., Jansen, G., Loos, M., Hättig, C. and Heß, B.A., *Chem. Phys. Lett.*, **219**, 267 (1994).
14. Muetterties, E.L., *"The chemistry of boron and its compounds"*, (Wiley, New York, 1967).
15. Pitzer, K.S., *J. Am. Chem. Soc.*, **77**, 3427 (1955).
16. Dymond, J.H. and Smith, E.B., *"The virial coefficients of pure gases and mixtures"*, (Oxford University Press, Oxford, 1980).
17. Bishop, D.M. and Cheung, L.M., *J. Phys. Chem.*, **11**, 119 (1982).
18. Lowery, H., *Proc. Roy. Soc. A.*, **133**, 188 (1931).
19. Watson, H.E. and Ramaswamy, K.L., *Proc. Roy. Soc. A*, **156**, 144 (1936).
20. Maryott, A.A. and Buckley, F , *"Table of dielectric constants and electric dipole*

moments of substances in the gaseous state.", (National Bureau of Standards, Washington, 1953).

21. Lamb, D.W. and Ritchie, G.L.D., unpublished results.
22. Gordy, W. and Cook, R.L., *'Microwave molecular spectra"*, (John Wiley, New York, 1984).
23. Dougherty, J. and Spackman, M.A., *Mol. Phys.*, **82**, 193 (1994).
24. Kellö, V. and Sadlej, A.J., *J. Chem. Phys.*, **93**, 8122 (1990).
25. Kellö, V. and Sadlej, A.J., *Mol. Phys.*, **75**, 209 (1992).
26. Watson, J.N., *"The measurement of field-gradient induced birefringence in gases"*, Ph.D. Thesis, University of New England, (1994).
27. Vrbancich, J. and Ritchie, G.L.D., *J. Chem. Soc. Faraday Trans. 2*, **76**, 648 (1980).
28. Bauschlicher Jr, C.W. and Ricca, A., *Chem. Phys. Lett.*, **237**, 14 (1995).
29. Glendening, E.D. and Streitwieser, A., *J. Chem. Phys.*, **100**, 2900 (1994).

Chapter Five

Benzene, toluene, *o*-xylene, *m*-xylene, *p*-xylene and mesitylene

Introduction

The electric properties of the fluorobenzenes have been investigated using the Kerr effect [1-3]. The change in the mean polarizability as a function of the number of fluorine atoms substituted into the benzene ring was found to be negligible, and this is a well known observation. A small, but nevertheless regular increase in the magnitude of the in-plane components and the polarizability anisotropy, and a similarly small decrease in the out-of-plane components, was noted. The success of the description of the electric properties of the fluorobenzenes was a motivation to undertake a systematic investigation of the methyl-substituted benzenes. Solution-phase Kerr effect experiments [4] have been reported for some of the methylbenzenes. Gas-phase Kerr effect measurements [3] of the xylenes have yielded inconclusive results due to the small temperature dependent term (equation 1.30). The results presented in this chapter are the Rayleigh depolarization ratios for benzene toluene, *o*-xylene, *m*-xylene, and *p*-xylene. The analysis is limited to a determination of $\Delta\alpha$ (or $|3\alpha\kappa|$) for each molecule. Literature values are included for mesitylene to permit a comparison of the electric properties of the methylbenzenes.

Experimental details

Samples of toluene (> 97.5%), *o*-xylene (> 99%), *m*-xylene (> 99%) and *p*-xylene (> 98.5%) were obtained from BDH Ltd. The samples were purified using

procedures given in the literature [5]. Gas-chromatographic analyses gave the final purities as *o*-xylene (> 99.5%), *m*-xylene (> 99.85%), *p*-xylene (> 99.95%), and toluene (> 99.5%). Benzene (> 99.99%), obtained from the Aldrich Chemical Company, was used without further purification. The depolarization ratios obtained in this study are given in Table 5.1, and were recorded using Versions 1 and 2 of the apparatus with inclusion of the vibrational Raman lines. Due to the relatively low volatility of all the methyl-substituted benzenes, temperatures of 80 to 90 °C were used to obtain the depolarization ratios, and mean polarizabilities were not determined.

A summary of typical values of the temperatures, pressures, count rates, and integration times is given in Table 5.2 for all species. For *o*-xylene, the ratios obtained with Version 2 of the apparatus were approximately 2% higher than those obtained with Version 1. At the time of these measurements, the depolarization ratios for carbon dioxide were $100\rho_0 = 4.00 \pm 0.05$ for Version 1 and $100\rho_0 = 4.04 \pm 0.05$ for Version 2. Since these were within 1% of each other, the ratios for *o*-xylene were not scaled. The ratios for *m*-xylene measured with Version 2 of the apparatus were 1.5% higher than the ratios measured with Version 1. At the time of these measurements, the depolarization ratios for carbon dioxide were $100\rho_0 = 4.01 \pm 0.02$ and $100\rho_0 = 4.03 \pm 0.02$ for Versions 1 and 2, which was a 0.5% difference. This does not account for the slightly higher ratio found with Version 2, but the uncertainties are large enough for any scaling of the data to be unnecessary. For *p*-xylene, there was excellent agreement amongst the ratios obtained with both versions, and therefore only two ratios were recorded with Version 2 of the apparatus. This was reflected in the agreement between the carbon dioxide depolarization ratios of $100\rho_0 = 4.03 \pm 0.02$ for Version 1 and $100\rho_0 = 4.04 \pm 0.02$ for Version 2.

Discussion

A summary of the depolarization ratios, mean polarizabilities and polarizability anisotropies is given in Table 5.3. The depolarization ratio for mesitylene was obtained from Hesling [6]. The mean polarizabilities were obtained from liquid-phase refractive

Table 5.1 Depolarization ratios for benzene, toluene, *o*-xylene, *m*-xylene and *p*-xylene.

$100\rho_0$				
benzene	toluene	*o*-xylene	*m*-xylene	*p*-xylene
1.889 ± 0.004[a]	1.845 ± 0.004	1.792 ± 0.007	1.823 ± 0.005	2.230 ± 0.007
1.889 ± 0.004[a]	1.878 ± 0.004	1.789 ± 0.007	1.845 ± 0.006	2.163 ± 0.007
1.891 ± 0.004[a]	1.855 ± 0.004	1.793 ± 0.007	1.869 ± 0.006	2.148 ± 0.007
1.906 ± 0.004[a]	1.848 ± 0.004	1.796 ± 0.007[a]	1.864 ± 0.006	2.187 ± 0.005
	1.885 ± 0.005	1.886 ± 0.009[a]	1.856 ± 0.006	2.190 ± 0.007
	1.891 ± 0.005	1.813 ± 0.006[a]	1.88 ± 0.01[a]	2.152 ± 0.007
		1.856 ± 0.006[a]	1.90 ± 0.01[a]	2.179 ± 0.005[a]
		1.825 ± 0.005[a]	1.87 ± 0.02[a]	2.18 ± 0.01[a]
		1.814 ± 0.005[a]	1.90 ± 0.01[a]	
		1.839 ± 0.005[a]		

[a] Values were recorded with Version 2 of the apparatus.

Table 5.2 Summary of typical experimental variables for benzene, toluene, *o*-xylene, *m*-xylene, *p*-xylene and mesitylene.[a]

	benzene	toluene	*o*-xylene	*m*-xylene	*p*-xylene
T (°C)	90	(81.6)	86.8	86.9	86.8
			(80.7)	(80.3)	(81.6)
p (kPa)	35	(19.3)	11.7	12.1	11.7
			(5.75)	(6.01)	(7.12)
depolarized count (cps)	1 522	(666)	1187	446	1260
			(230)	(279)	(374)
polarized count (cps)	79 640	(35 170)	64 819	22 820	57 570
			(12 600)	(14 700)	(16 566)
depolarized background count (cps)	5	(6)	5 (4)	17 (4)	6 (5)
polarized background count (cps)	64	(12)	22 (14)	66 (16)	20 (19)
depolarized integration time (s)	200	(1 000)	400 (1 000)	500 (1 000)	400 (1 000)
polarized integration time (s)	100	(500)	200 (500)	250 (500)	200 (500)

[a] Values given in parentheses are for Version 1 of the apparatus.

indicies interpolated for 632.8 nm [7-9]. The uncertainty in the mean polarizabilities was estimated to be ± 2% to account for the quadratic least-squares analysis, and for slight differences between the literature data.

The depolarization ratio of benzene is considered to be very reliable and it agrees with values obtained by Alms *et al.* [10], Bogaard *et al.* [11] and Hesling [6]. A better value for the mean polarizability of benzene would be 11.56 (and hence $\Delta\alpha = -6.23$) as quoted by Bogaard *et al.* [11] and Kumar and Meath [12] from refractive indices and dipole oscillator-strength distributions, respectively. The liquid-phase value is included in the calculations for consistency with the other molecules in the series. The liquid-phase refractive indicies for benzene and toluene have been confirmed [13].

The vapour-phase depolarization ratios of benzene at 30 °C, toluene at 40 °C and the xylenes at 60 °C have been determined by Panachev *et al.* [14,15], and the results are given in Table 5.3 for comparison Assuming the present ratios are accurate, then the ratios reported by Panachev *et al.* are too low, despite what seems to be excellent agreement. For example, the benzene ratio of 1.90 ± 0.03 reported by Panachev *et al.* is in agreement with the present value, but the result is for a wavelength of 488.0 nm. Therefore, the ratio should be lower when interpolated to 632.8 nm, due to dispersion. This puts in doubt the results for *o*-, *m*-, and *p*-xylene as well. The toluene ratio reported by Panachev *et al.* is higher than the present result, and this can probably be attributed to dispersion.

The values of $\Delta\alpha$ (or $|3\alpha\kappa|$) reported in Table 5.3 give a measure of the effect of methyl substitution into the benzene ring. The polarizability anisotropy for toluene is an increase of ≈ 20% with respect to benzene. This is probably due to an increase of the in-plane polarizability along the 1,4-axis, which is also reflected in an increase of the mean polarizability. The effect of a second methyl group substituted into the benzene ring is to increase the anisotropy by ≈ 35 to 50% with respect to benzene, depending on the molecule. Since the uncertainties are large for the mean polarizabilities of the xylenes, it is concluded that the change in the mean polarizability is not discernible. Substitution of a third methyl group increases the polarizability anisotropy by ≈ 50% with respect to the

Table 5.3 Depolarization ratios, mean polarizabilities and polarizability anisotropies of benzene, toluene, *o*-xylene, *m*-xylene, *p*-xylene and mesitylene.

	benzene	toluene	*o*-xylene	*m*-xylene	*p*-xylene	mesitylene
$100\rho_0$	1.894 ± 0.009^a	1.87 ± 0.02^a	1.82 ± 0.03^a	1.87 ± 0.03^a	2.18 ± 0.03^a	1.80 ± 0.05^b
	1.90 ± 0.03^c	1.95 ± 0.02^c	1.81 ± 0.03^c	1.89 ± 0.04^c	2.22 ± 0.02^c	
α^d	11.49 ± 0.22	13.65 ± 0.28	15.72 ± 0.32	15.79 ± 0.32	15.81 ± 0.32	17.92 ± 0.36
$\Delta\alpha^e$	-6.20 ± 0.12	(7.32 ± 0.16)	(8.31 ± 0.18)	(8.47 ± 0.18)	(9.17 ± 0.20)	-9.43 ± 0.23

a Present study, vibrational Raman lines included.

b From gas-phase Rayleigh light scattering measurements for 632.8 nm [6].

c From gas-phase Rayleigh light scattering measurements for 488.0 nm [14,15].

d Derived from liquid-phase refractive indices interpolated for 632.8 nm [7-9].

e Values in parentheses are $|3\alpha\kappa|$.

benzene ring. This is due to an increase in the in-plane polarizabilities, and this is again reflected in an increase in the mean polarizability. Overall, the contribution of methyl groups to the mean polarizabilities is additive, since each additional group contributes approximately 2.1 to the total polarizability. This is slightly less than half of the mean polarizability of ethane (Chapter 6). The dependence of α and $\Delta\alpha$ on the number of methyl groups substituted into the benzene ring is given in Figure 5.1. From the figure, it is clear that the dependence is linear for both α and $\Delta\alpha$, although the value of $\Delta\alpha$ for *p*-xylene is slightly high; this is due to the methyl groups increasing the ellipticity, and therefore the anisotropy, of the molecule.

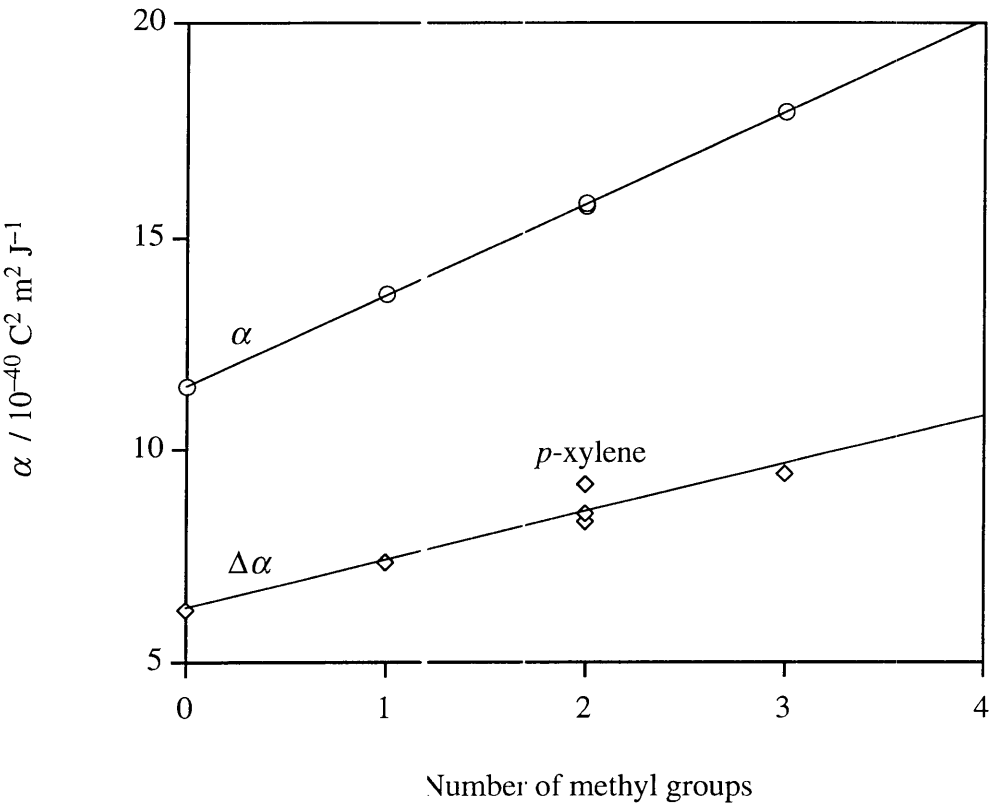

Figure 5.1 Dependence of α and $\Delta\alpha$ on the number of methyl groups for molecules in the sequence benzene, toluene, *o*-xylene, *m*-xylene, *p*-xylene, and mesitylene.

As mentioned in the introduction, gas-phase Kerr effect studies of the xylenes, to date, have yielded inconclusive results [3]. From equation 1.32, it is evident that a plot of $\left[A_K - N_A\gamma^K/81\varepsilon_0\right]T$ against T^{-1} gives a temperature dependent component of

$N_A\mu^2(\alpha_{zz}-\alpha)/270k^2\varepsilon_0$. For the xylenes the dipole moments are relatively small, so that the above term is difficult to determine precisely. To derive the three principal polarizabilities of each molecule, the values of $\alpha_{zz}-\alpha$ can be combined with the values of κ^2 obtained from the present light scattering results (equation 1.8), and the known mean polarizabilities, giving the equation

$$\kappa^2=\left[\left(\alpha_{xx}-\alpha_{yy}\right)^2+\left(\alpha_{yy}-\alpha_{zz}\right)^2+\left(\alpha_{zz}-\alpha_{xx}\right)^2\right]/18\alpha^2 \qquad (5.1)$$

The quadratic nature of this equation results in two solutions for the set of polarizabilities. Usually the choice between the two sets is unambiguous; however, the results for the xylenes are not well-defined and have given, in at least one case, physically unreasonable quantities or insoluble equations.

Solution-phase Kerr effect measurements of benzene, toluene, *p*-xylene, and mesitylene in cyclohexane have been reported by Aroney and Pratten [4]. Solution-phase measurements usually result in an underestimate of the polarizability anisotropy. The theory does not account for local-field effects from neighbouring solute and solvent molecules, and contributions from the Kerr hyperpolarizabilities are usually unknown and assumed to be negligible [2]. For example, the value of $\Delta\alpha$ = –4.6 for benzene reported by Aroney and Pratten is 25% less than the currently accepted value of –6.2. Despite these shortcomings, the solution-phase work does reproduce the linear dependence of α and $\Delta\alpha$ on the number of methyl groups substituted into the benzene ring.

A systematic study of other substituted benzenes such as the chloro- and bromo-benzenes, the phenols, and the anilines is limited by the low volatility of these compounds. For example, the present Rayleigh light scattering and Kerr effect equipment within this research group have maximum operating temperatures of 120 and 240 °C, respectively. The monosubstituted chlorobenzenes and bromobenzenes have boiling points of 132 and 156 °C, respectively. Therefore, it should be possible to study these molecules, although a study of the temperature dependence of the Kerr effect would

be severely limited. The disubstituted and trisubstituted species, however, have boiling points above 200 °C and are therefore outside the temperature ranges of the present apparatus.

Conclusions

The depolarization ratios for benzene, toluene and the xylenes were determined. The ratio for benzene was found to be in excellent agreement with the literature values. The depolarization ratios for benzene and the xylenes were found to disagree with the values reported by Panachev *et al.* [14,15]. Mean polarizabilities obtained from the literature were combined with the depolarization ratios to determine the $\Delta\alpha$ (or $|3\alpha\kappa|$) values. The mean polarizabilities and polarizability anisotropies of benzene, toluene, the xylenes, and mesitylene were found to depend linearly on the number of methyl groups substituted into the benzene ring.

References

1. Gentle, I.R., Hesling, M.R. and Ritchie, G.L.D., *J. Phys. Chem.*, **94**, 1844 (1990).
2. Gentle, I.R. and Ritchie, G.L.D., *J. Phys. Chem.*, **93**, 7740 (1989).
3. Blanch, E.W. and Ritchie, G.L.D., unpublished results.
4. Aroney, M.J. and Pratten, S.J., *J. Chem. Soc., Faraday Trans. 1*, **80**, 1201 (1984).
5. Perrin, D.D., Armarego, W.L.F. and Perrin, D.R., *"Purification of laboratory chemicals"*, 2nd Edition (Pergamon, Oxford, 1980).
6. Hesling, M.R., *"Measurements of Rayleigh depolarization ratios of gases and vapours."*, Ph.D. Thesis, University of New England, (1990).
7. Forziati, A.F. and Rossini, F.D., *J. Res. Nat. Bur. St.*, **43**, 473 (1949).
8. Forziati, A.F., *J. Res. Nat. Bur St.*, **44**, 373 (1950).
9. Petro, A.J. and Smyth, C.P., *J. Am. Chem. Soc.*, **80**, 73 (1958).
10. Alms, G.R., Burnham, A.K. and Flygare, W.H., *J. Chem. Phys.*, **63**, 3321 (1975).
11. Bogaard, M.P., Buckingham A.D., Pierens, R.K. and White, A.H., *J. Chem. Soc., Faraday Trans. 1*, **74**, 3008 (1978).
12. Kumar, A. and Meath, W.J., *Mol. Phys.*, **75**, 311 (1992).
13. LeGrand, G.G. and Gaines Jr, G.L., *J. Phys. Chem.*, **98**, 4842 (1994).
14. Panachev, F.I., Korableva, E.Y. and Shakhaparonov, M.I., *Russ. J. Phys. Chem.*, **50**, 1130 (1976).
15. Panachev, F.I. and Korableva, E.Y., *Russ. J. Phys. Chem.*, **51**, 943 (1977).